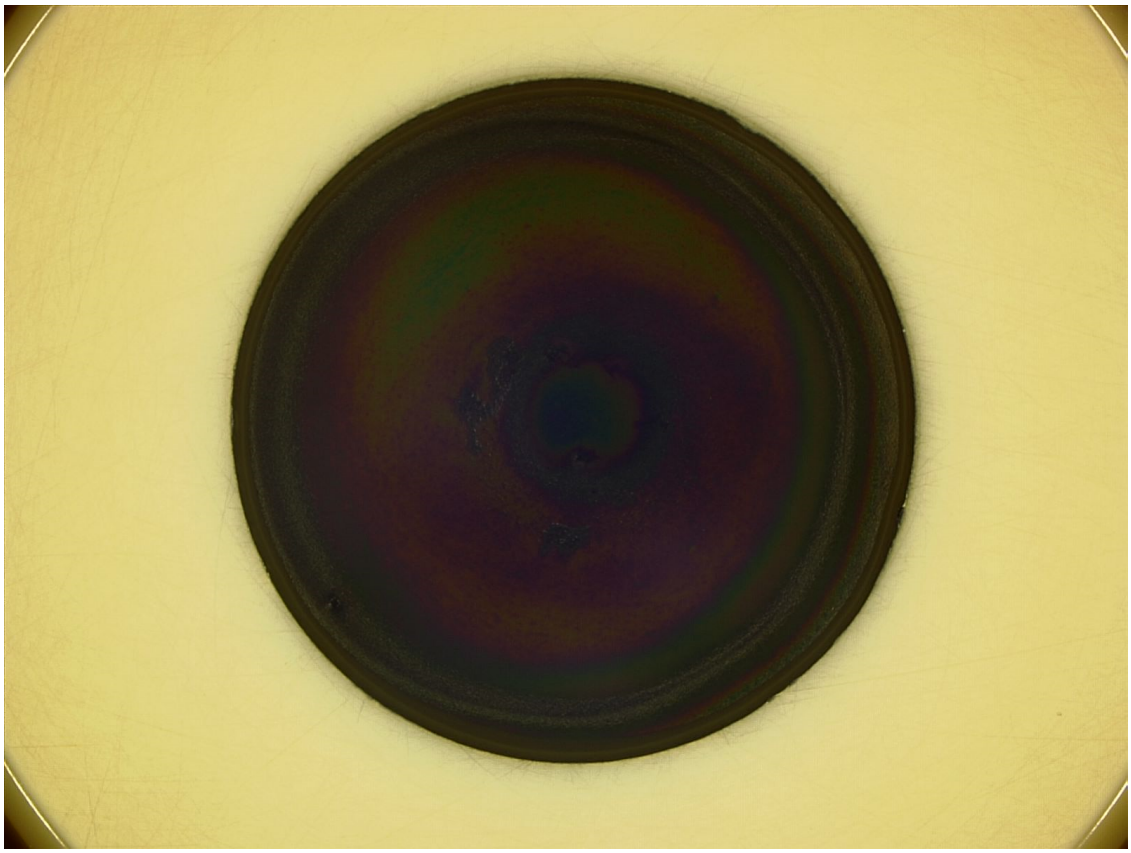

Fuel cell catalyst coating quality for reliable ex-situ ORR activity results

Master's thesis in Physics

HUGO MÅRTENSSON

DEPARTMENT OF PHYSICS

CHALMERS UNIVERSITY OF TECHNOLOGY
Gothenburg, Sweden 2025
www.chalmers.se

Master's thesis 2025

Fuel cell catalyst coating quality for reliable ex-situ ORR activity results

HUGO MÅRTENSSON

CHALMERS
UNIVERSITY OF TECHNOLOGY

Department of Physics
Division of Chemical Physics
Chalmers University of Technology
Gothenburg, Sweden 2025

Fuel cell catalyst coating quality for reliable ex-situ ORR activity results
HUGO MÅRTENSSON

Supervisor: Marika Männikkö, PowerCell Group AB
Examiner: Björn Wickman, Department of Physics

Master's Thesis 2025
Department of Physics
Division of Chemical Physics
Chalmers University of Technology
SE-412 96 Gothenburg
Telephone +46 31 772 1000

Cover: Pt/C catalyst on a glassy carbon electrode.

Typeset in LaTeX
Gothenburg, Sweden 2025

Fuel cell catalyst coating quality for reliable ORR activity results
HUGO MÅRTENSSON
Department of Physics
Chalmers University of Technology

Abstract

Proton exchange membrane fuel cells (PEMFCs) are energy conversion devices that could play a key role in the reduction of greenhouse gas emissions. However, one major problem for PEMFCs is the slow oxygen reduction reaction (ORR), which causes large overpotentials and requires a large amount of expensive platinum catalyst to be sped up. For that reason, evaluation of the ORR activity of catalysts is important, and the rotating disk electrode (RDE) method is commonly used for this purpose. However, there are still problems with achieving reliable results of the ORR activity with RDE, specifically due to the activity's dependence on the quality of the catalyst coating on the electrode. This thesis investigates how different parameters of a catalyst ink influence the catalyst coating and how to achieve a uniform thin coating. For one catalyst, inks with different alcohol contents and platinum loadings were tested, and for a second catalyst, different alcohol contents and pH levels were tested.

The alcohol content did not appear to have a significant impact on the ORR activity or the homogeneity of the thin films. A high alcohol content facilitated the spreading out of the ink due to a lower surface tension, but it was also harder to keep it from spreading outside the electrode disk. With platinum loading, there seemed to be a lower limit between 10 and 20 $\mu g_{Pt}/cm^2$ for the catalyst to cover the entire disk homogenously. Below this limit, the mean specific ORR activity was about 20% lower. At 34.8 $\mu g_{Pt}/cm^2$, the results were about the same as for 20 $\mu g_{Pt}/cm^2$, meaning no upper limit appears to have been reached. For the second catalyst, stability issues were observed, which did not significantly change with the alcohol content. Increasing the pH of the ink by adding KOH improved ink stability, but it was still not possible to produce a completely homogeneous coating. Further investigations on how to achieve a homogeneous coating with this catalyst are therefore needed.

Keywords: Proton exchange membrane fuel cell, oxygen reduction reaction, rotating disk electrode, Pt/C catalyst.

Acknowledgements

First and foremost, I would like to thank my supervisor Marika Männikkö, for her continuous feedback and guidance throughout this entire work. I would also like to thank PowerCell Group AB for the possibility of performing my master's thesis there, as well as my collegues there for their support and good company. A special thanks to Caroline Sundbye for her help with introducing the experimental parts of the work. Lastly, a big thanks to my examiner Björn Wickman for his support and feedback.

Hugo Mårtensson, Gothenburg, June 2025

List of Acronyms

Below is the list of acronyms that have been used throughout this thesis listed in alphabetical order:

CE	Counter electrode
CV	Cyclic voltammetry
EIS	Electrochemical impedance spectroscopy
ECSA	Electrochemical surface area
KOH	Potassium hydroxide
GC	Glassy carbon
IPA	2-propanol
MA	Mass activity
MEA	Membrane electrode assembly
ORR	Oxygen reduction reaction
PEMFC	Proton exchange membrane fuel cell
Pt	Platinum
Pt/C	Platinum on a carbon support
RDE	Rotating disk electrode
RE	Reference electrode
RHE	Reversible hydrogen electrode
SA	Specific activity
WE	Working electrode

Contents

List of Figures

List of Tables

1

Introduction

Global warming is one of the many challenges our society faces today. Emissions of carbon dioxide and other green house gases need to be reduced in order to accomplish the goal of the Paris Agreement, to limit global warming to 1.5 °C above pre-industrial levels [1]. This requires development of new technologies to convert energy more efficiently with low, possibly zero, emissions. Besides its emissions of carbon dioxide, fossil fuels are finite, which means it is obvious that other alternative energy sources need to be used in the long term [2]. Fuel cells presents one piece of the solution to these problems. They are efficient energy converters that based on electrochemical principles, convert chemical energy stored in a fuel directly to electricity. What fuel is used differs, but hydrogen, methane and methanol are some examples [2]. It is possible to produce hydrogen through renewable means and by combining water electrolysis, storage of hydrogen gas and fuel cells, it provides a possible solution to the intermittency that plagues renewable energy sources such as wind and solar.

A fuel cell is similar to a battery. It has a negative and a positive electrode, separated by an electrolyte and through the use of redox reactions at these electrodes, a DC current is generated. In contrast to a battery, a fuel cell requires a constant flow of fuel and oxidant to operate and its electrodes do not change as part of the redox reactions. A battery on the other hand stores energy and generates a current by using material already inside it. It will continue to operate only for as long as there is material in the battery to undergo the electrochemical reactions, until the battery is completely discharged. A fuel cell cannot be discharged, it will continue to output electricity for as long as fuel and oxidant are supplied (disregarding degradation). There will also be by-products generated by a fuel cell, often water and heat, that need to be handled, although the heat could be used in some way. A battery also produces heat, but not to the same extent [3].

Fuel cell technology has been around for some time, with the first fuel cell being developed in 1842, with its first practical application being a part of the U.S. space program in the 1960s [3]. Today, fuel cells show great promise as a possible solution to global warming but there exists some obstacles, for example degradation and the price of the catalyst. Catalysts are used in fuel cells to increase the rate of the electrochemical reactions. The material used as a catalyst in proton exchange membrane fuel cells (PEMFCs), a popular type of fuel cell, is platinum, an expensive metal that makes up about half of the cost of a complete fuel cell stack [4]. The

sluggish kinetics of the cathode reaction in a PEMFC, the oxygen reduction reaction (ORR), requires a lot of catalytic material and is also the source for most of the losses in a fuel cell. Evaluating the ORR activity for new catalysts is therefore an important part in the continued development of new fuel cells. A common technique for this evaluation is the rotating disk electrode (RDE) method which allows for simple and inexpensive testing of catalysts ex situ. It also gives a meaningful prediction of the catalyst's performance in a fuel cell [5].

For the catalyst to be studied with the RDE method, a thin film of catalyst is coated on the electrode surface of the RDE. This is done by preparing an ink of catalyst and solvent and then depositing a small droplet of ink on the electrode. The ink is then dried such that it yields a smooth homogeneous film that covers the entire electrode surface. The difficulty of obtaining reproducible, comparable and accurate results of the ORR activity with the RDE method is however still an issue, even with many studies making efforts in increasing the method's reliability. In order to measure the ORR activity accurately, it is important that the film is of good quality. The film needs to be thin and uniform over the entire surface of the electrode and the quality is affected by the ink recipe and dispersion, drying conditions and electrode surface [6]. This thesis aims to study the influence of different catalyst ink parameters on the quality and reliability of ORR activity measurements.

1.1 Aim

The aim of this thesis is to increase the reliability of ORR activity measurements performed with the RDE method. This study focuses on investigating how a good quality film is produced, with a primary focus on different catalyst ink parameters. The influence of the water:alcohol ratios and platinum loadings on the coatings is examined. The quality of these coatings is evaluated visually with a light microscope and electrochemically with the RDE method. Additionally, the influence of the pH of catalyst inks on the quality of the coating is investigated.

1.2 Limitations

This thesis only studies the ORR activity ex-situ with the RDE technique. Other methods than light microscope and RDE to evaluate coatings are not used. Parameters of the RDE method such as electrolyte, rotation speed and scanning rate and range are not investigated. The scope is also be limited to two different commercial Pt/C catalysts, where Pt/C means platinum nanoparticles on a carbon support.

2

Theory

This chapter explains how fuel cells, and in particular proton exchange membrane fuel cells (PEMFCs), work. The theory behind the catalyst in a PEMFC, one of the main obstacles in the expanding commercialization of PEMFCs, is then covered as well as different techniques for characterizing PEMFC catalysts.

2.1 Fuel cells

A fuel cell is a device that generates energy from controlled and spontaneous oxidation and reduction reactions while being supplied with a fuel. It consists of two electrodes separated by an electrolyte, a material that conducts ions but not electrons. At one electrode, the anode, an oxidation reaction occurs and at the other electrode, the cathode, a reduction reaction occurs. The difference in Gibbs free energy between the reactions of the two electrodes drives the fuel cell and allows the extraction of electrical work. Electrons generated by the oxidation reaction are passed through an external circuit connecting the electrodes, creating useable electricity. The protons on the other hand are passed to the cathode through the ion conducting electrolyte. At the cathode, the protons and electrons are consumed in a reduction reaction. There are many different types of fuel cells which differ in their operation. A common fuel however is hydrogen, which together with oxygen from the air results in the fuel cell's only emissions being water and heat [7].

2.1.1 Proton exchange membrane fuel cell

A common type of fuel cell is the proton exchange membrane fuel cell (PEMFC). It offers advantages such as being compact, being able to output high power and to change the it rapidly, not including any hazardous liquid electrolytes and operating at relatively low temperatures [8]. PEMFCs work by converting the chemical energy in hydrogen into electricity. In a PEMFC, hydrogen is oxidized at the anode and oxygen from the air is reduced at the cathode, producing water and heat as the only emissions. Figure 2.1 shows a schematic diagram of a PEMFC. The hydrogen oxidation reaction (HOR) and oxygen reduction reaction (ORR), the anode and cathode reactions in a PEMFC, are

$$\text{Anode (HOR):} \qquad \mathrm{H_2} \longrightarrow 2\,\mathrm{H^+} + 2\,\mathrm{e^-} \tag{2.1}$$

$$\text{Cathode (ORR):} \qquad \mathrm{O_2} + 4\,\mathrm{H^+} + 4\,\mathrm{e^-} \longrightarrow 2\,\mathrm{H_2O}. \tag{2.2}$$

The overall reaction in a PEMFC is then

$$H_2 + \frac{1}{2} O_2 \longrightarrow H_2O. \tag{2.3}$$

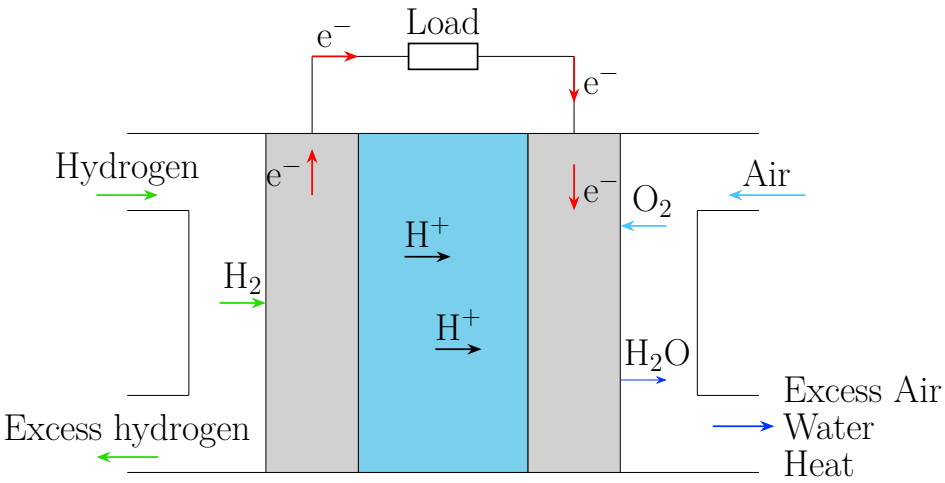

Figure 2.1: Schematic diagram of a PEMFC.

This is an exothermic reaction, meaning energy is released in the process. The energy, or enthalpy ΔH, of the reaction is difference in enthalpy of formation of the products and reactants, in this case $-286\,\mathrm{kJ/mol}$ at $25\,^\circ\mathrm{C}$ and atmospheric pressure [9]. Not all of this enthalpy can be converted to electricity however, due to losses caused by creation of entropy ΔS. The energy that can be converted to electricity is Gibbs free energy

$$\Delta G = \Delta H - T\Delta S \tag{2.4}$$

which in this case is $-237.34\,\mathrm{kJ/mol}$ [9]. The relationship between Gibbs free energy and the equilibrium cell voltage E_e is

$$\Delta G = -nFE_e \tag{2.5}$$

where n is the number of electrons needed to convert the reactant into product (in this case $n = 2$) and F is the Faraday constant. The Faraday constant is the charge of 1 mol of electrons, the product of Avogadro's number and the charge of one electron, and equals $96\,385\,\mathrm{C/mol}$ [8]. Using this equation, the theoretical potential of a PEMFC is 1.23 V. In reality it is lower than 0.9 V [10]. Several sources contribute to this loss of voltage, also known as overpotential, in different ways. They include kinetics of the electrochemical reactions, ohmic losses, internal currents and mass transport losses. Specifically, the slow kinetics of the oxygen reduction reaction is a major source of overpotential [11].

The heart of a PEMFC is the membrane electrode assembly (MEA). The MEA consists of a membrane, two electrodes and two gas-diffusion layers or diffusion media. Each side of the MEA is then connected to a bi-polar plate which transports

gases to and from the MEA. The hydrogen and oxygen are then transported to their respective electrodes by the porous gas diffusion layer [7].

Starting with the membrane, its role is to transport protons from the anode to the cathode, separate the oxygen and hydrogen gases, work as a support for the catalyst layer and be stable in the PEMFC environment. The conduction of protons needs to be done while minimizing the voltage drop which reduces the efficiency and power output of the cell. Mixing of hydrogen and oxygen gases should be avoided since it could lead to explosive reactions in the presence of a catalyst. To satisfy these criteria, the membrane consists of a thin film of a proton conductive polymer. This polymer includes covalent bonds to functional anionic groups which provides the proton conductivity [8].

Catalysts are used for both reactions in a PEMFC. However, the kinetics of the HOR is very fast and thus requires very little catalytic material. The ORR on the other hand, is significantly more sluggish and is the reason for most of the losses in a PEMFC. The catalyst used in the electrodes of a PEMFC is usually platinum (Pt), or a platinum alloy, in the form of nanoparticles on a carbon support. However, even with a platinum catalyst, the ORR suffers from high overpotentials [7].

2.1.2 Other types of fuel cells

There exists many types of fuel cells in addition to PEMFCs. For example phosphoric acid fuel cells (PAFC) that operate at higher temperatures compared to PEMFCs, about 160 – 200 °C, and was one of the first fuel cell technologies. The redox reactions are similar to those in a PEMFC but the electrolyte is concentrated phosphoric acid absorbed into a SiC paste [7]. The catalyst is also similar to that in a PEMFC, platinum on a carbon support. Its higher operating temperature allows for faster kinetics of the ORR and reduced CO poisoning at the anode [8], a phenomenon caused by CO strongly adsorbing to the platinum surface. PAFCs are used mostly for stationary power plants [7].

Another type of fuel cell is molten-carbonate fuel cells (MCFCs) which operate at much higher temperatures, 600 – 700 °C, in order for the electrolyte to reach a good enough conductivity. The electrolyte is made up of a molten salt (K_2CO_3/Li_2CO_3 or Na_2CO_3/Li_2CO_3) that is absorbed in a ceramic matrix. Because of the high operating temperature, MCFCs do not need precious metals as catalysts and can for example use Ni-Cr alloy at the anode and NiO at the cathode. The anode and cathode reactions in an MCFC is

$$\begin{aligned} &\text{Anode:} && H_2 + {CO_3}^{2-} \longrightarrow H_2O + CO_2 + 2\,e^- \\ &\text{Cathode:} && \frac{1}{2}\,O_2 + CO_2 + 2\,e^- \longrightarrow {CO_3}^{2-}. \end{aligned}$$

The high temperature makes the anode resistant to CO poisoning but also increases corrosion and degradation of the cathode [7].

There are also fuel cells that use a solid electrolyte, so called solid oxide fuel cells (SOFCs). The electrolyte of a SOFC is a non-porous metal oxide or ceramic which

requires a high temperature to allow ion conduction. The operating temperature of an SOFC is therefore in the range 600 – 1000 °C [7] which allows it to use fossil fuels such as hydrocarbons directly, due to reforming at the electrocatalyst layer [8]. For the catalysts, Lanthanum strontium manganite is used at the cathode while the anode uses Ni combined with the electrolyte material. The redox reaction at the cathode in an SOFC is

$$O_2 + 4\,e^- \longrightarrow 2\,O^{2-}$$

and at the anode

$$H_2 + O^{2-} \longrightarrow H_2O + 2\,e^-$$

but the anode reaction could differ depending on the fuel used [8].

The last type of fuel cells that will be mentioned here are alkaline fuel cells (AFCs). These fuel cells use potassium hydroxide as the electrolyte. Advantages of a AFC include lower overpotential losses of the oxygen reduction reaction compared to fuel cells with acid electrolytes, as well as being able to use non-precious metals as catalysts. The redox reactions that occur in an AFC are

$$\begin{aligned} &\text{Anode:} && 2\,H_2 + 4\,OH^- \longrightarrow 4\,H_2O + 4\,e^- \\ &\text{Cathode:} && O_2 + 2\,H_2O + 4\,e^- \longrightarrow 4\,OH^-. \end{aligned}$$

These fuel cells are however very sensitive to CO_2 which forms solid K_2CO_3, lowering the ionic conductivity of the electrolyte and blocking electrode pores [7].

2.1.3 Oxygen reduction reaction

The oxygen reduction reaction (ORR) occurs at the cathode of a fuel cell and its slow kinetics is one of the main reasons for the difficulty of commercializing fuel cell technology. As mentioned earlier, the ideal voltage of a fuel cell is 1.23 V but the observed voltage is lower than 0.9 V. This overpotential is primarily caused by the ORR but the exact reasons are unclear because of the reaction's complexity [10].

An overpotential is a difference between the electrode potential and the equilibrium potential and is needed in order to generate a current. The relationship between the overpotential and the current is described by the Butler–Volmer equation

$$i = i_0 \left(\exp\left[\frac{\alpha_{Ox} n F (E - E_e)}{RT} \right] - \exp\left[\frac{-\alpha_{Red} n F (E - E_e)}{RT} \right] \right) \tag{2.6}$$

where i_0 is the exchange current density, meaning the reaction rate at equilibrium, α is a transfer coefficient and n is the number of electrons involved in the electrode reaction [11]. The overpotential is $E - E_e$, the difference between the applied potential and the equilibrium potential. The Butler–Volmer equation can describe both the HOR and ORR but the sign of their respective overpotentials will be different. For the cathode, $E < E_e$, which makes the first term negligible compared to the second. The dominant current will then be the reduction current. At the anode, the opposite is true since $E > E_e$, making the dominant current the oxidation current [11].

The voltage loss caused by the overpotential is called activation polarization and is related to sluggish electrode kinetics. Even though this is relevant for both the HOR and ORR, the sluggish kinetics of the ORR requires much higher overpotentials. The activation polarization can be expressed as a function of current density by utilizing the second term of the Butler–Volmer equation which is dominant at high overpotentials [11]. This yields

$$\Delta V_{act} = \frac{RT}{\alpha n F} \ln\left(\frac{i}{i_0}\right). \tag{2.7}$$

Comparing the exchange current density i_0 between the HOR and ORR, i_0 is of the order $10^{-3}\,\mathrm{A/cm^2}$ for the HOR and $10^{-8}\,\mathrm{A/cm^2}$ for the ORR [2]. The activation polarization can be further simplified with the Tafel equation

$$\Delta V_{act} = a + b \log i \tag{2.8}$$

where $b = 2.3RT/\alpha nF$ is called the Tafel slope. A typical value for the ORR on Pt is $60\,\mathrm{mV}$ per decade which is the value when $\alpha n = 1$ and $T = 60\,^{\circ}\mathrm{C}$ [11].

The exact cause for the high overpotential is still unclear even after extensive research and the ORR is a complex reaction with many intermediate steps [10]. There are two ways for oxygen to be reduced [8]. The first one is a direct four-electron pathway without any intermediates,

$$\mathrm{O_2} + 4\,\mathrm{H^+} + 4\,\mathrm{e^-} \longrightarrow \mathrm{H_2O}, \tag{2.9}$$

and the other one is a two-electron driven reaction where $\mathrm{H_2O_2}$ is formed:

$$\mathrm{O_2} + 2\,\mathrm{H^+} + 2\,\mathrm{e^-} \longrightarrow \mathrm{H_2O_2}. \tag{2.10}$$

In the ORR mechanism, the rate limiting step is identified as $\mathrm{O_2}$ being dissociated and adsorbed onto the platinum surface. The dynamics of the ORR is heavily influenced by the catalyst and even though many metals could be used, platinum and combinations of platinum with other metals are considered to be among the most promising candidates. The structural and electronic properties of platinum based catalysts make them able to destabilize intermediates which reduces the activation energy barrier and thus increases the kinetic rate of the ORR [10].

2.2 Catalysts for proton exchange membrane fuel cells

Catalysts are used in fuel cell in order to increase the rate of the reactions occurring. The structural och electronic properties of the catalytic material make them able to destabilize intermediates of the reactions, which leads to a reduced energy barrier. Reducing the energy barrier of the reaction increases the kinetic rate of which that

reaction occurs [10]. Today, the catalyst commonly used in both the anode and cathode electrode of a PEMFC is platinum (or a platinum alloy) nanoparticles on a carbon support (Pt/C). The size of the nanoparticles is usually in the range of 2 – 4 nm but it could depend on the support used, alloying and heat treatment of the catalyst [7].

By using Gibbs free energy to calculate the binding energy of the intermediates in each step of the ORR, the activity can be plotted versus the binding energy for different metals. If the binding energy is too high, O and OH binds to strongly to the metal and the proton transfer step will be slow. If O and OH binds too loosely to the metal, there is no transfer of protons and electrons to the oxygen. This creates a volcano like plot, with Pt on the top, meaning it has the highest activity compared to other metals [12].

The high surface area to volume ratio of nanoparticles allows the catalyst to achieve high catalytic activity while keeping the loading of platinum low. A support material also hinders agglomeration of Pt nanoparticles when the concentration of Pt is increased, which is good since agglomeration decreases the surface area and thus activity of the Pt. For ORR, Pt/C is recognized as one of the most promising catalysts. Many properties of the carbon support like small particles, high surface area, uniform morphology, highly dispersed and good interactions with the Pt contribute to an increased Pt utilization [13].

However, a problem with a carbon support is that it oxidizes during the operation of a PEMFC, something which especially occurs during start up and shut down of the PEMFC. During these processes, the potential is higher compared to steady state conditions, which speeds up the corrosion of the carbon. When the carbon oxidizes, it forms carbon dioxide (or carbon monoxide at even higher potentials), weakening the interaction between the Pt nanoparticles and the carbon support. A weakened bonding interaction causes the Pt particles to separate from the support and agglomerate [14]. Finding a non-corrosive support that enhances the catalytic activity and durability is therefore an active area of research [13].

2.3 Electrochemical techniques

This section introduces the electrochemical techniques that are used to characterize fuel cell catalysts and explains how the ORR activity is determined with the RDE method.

2.3.1 Three-electrode cell

Electrochemical studies are often performed in three-electrode cells. A three electrode cell consists of a working electrode (WE), counter electrode (CE) and reference electrode (RE), submerged in an electrolyte as shown in Figure 2.2. Between the WE and CE, a current is passed, while no (or a small) current is passed through the RE. The RE is used as a reference when controlling the potential of the WE [15], which is the electrode that is studied. It should be the chemistry of the WE that

determines the experimental data from a measurement in a three-electrode cell. The material of the WE can vary greatly depending on the study but this thesis uses a thin film of Pt/C catalyst coated on a glassy carbon (GC) disk. For the CE, its objective is to provide a current with the same magnitude but different sign as the current at the WE. This should occur without affecting the response of the WE [8].

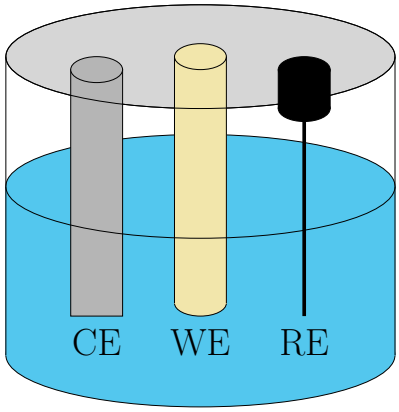

Figure 2.2: Schematic diagram of a three-electrode cell.

Since the job of the RE is to provide a reference for controlling the potential of the WE, it is important that the potential of the RE remains constant during the experiment and does not vary between measurement days. A basic RE is the standard hydrogen electrode (SHE) which consists of a high area platinum electrode in a 1 M proton solution and is saturated with hydrogen. It is defined by the equilibrium potential of

$$H^+ + e^- \longleftrightarrow \frac{1}{2} H_2 \tag{2.11}$$

at standard conditions. When the pH of the solution is no longer 0, the same RE is a reversible hydrogen electrode (RHE), which deviates from the SHE based on the pH level [16].

2.3.2 Cyclic voltammetry

In cyclic voltammetry (CV), the potential of the WE is swept between two values while the current is measured. The potential starts at one value and changes linearly until it reaches the other value, where the sweep direction is reversed and the potential goes back to the first value [17]. This is one cycle.

A typical cyclic voltammogram for a Pt/C catalyst in an inert environment is shown in Figure 2.3. There are four main reactions that happen in this cycle. When decreasing the potential from the highest value, the first reaction that occurs is the reduction of platinum. Then at lower potentials, there is hydrogen adsorption on the platinum. When the sweep direction is reversed and the potential increasing, the hydrogen is desorbed and then the platinum oxidizes [18]. An electric double layer is also visible as the flat region between the hydrogen adsorption/desorption and Pt reduction/oxidation, at about 0.4 – 0.5 V vs. RHE. When a potential is applied

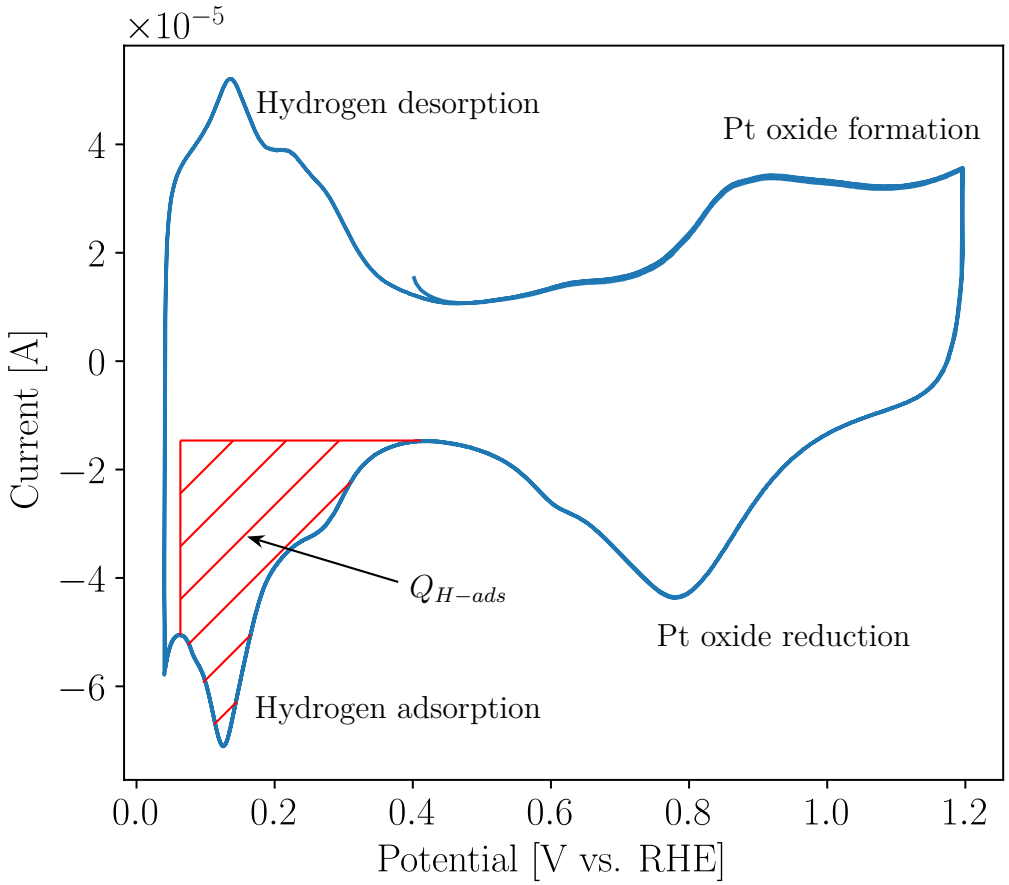

Figure 2.3: A typical voltammogram with the area used to calculate the ECSA highlighted.

to the electrode, it takes up a characteristic charge. This charge attracts ions of opposite charge, forming an electrical double layer. The electrical double layer can be characterized with a capacitance defined by the change in charge as the potential changes. For CV, the current density will be the product of this capacitance and the scanning rate when no Faradaic processes occur, meaning no current is generated by reduction or oxidation [8].

With the help of a CV measurement, one can calculate the electrochemical surface area (ECSA). The ECSA is an important parameter of the catalyst and is used when determining the area-specific ORR activity. Both the hydrogen adsorption and desorption areas of the voltammogram can be used to calculate the ECSA, but in this thesis it is calculated using the adsorption charge. The hydrogen adsorption charge Q_{H-ads} is calculated by integrating the part of the voltammogram that corresponds to the hydrogen adsorption [6], since

$$Q = \int I \mathrm{d}t. \tag{2.12}$$

The integration is done over the red area in Figure 2.3 but with the x-axis converted

to time. The baseline for the integration is such that current stemming from the electrical double layer is excluded. After obtaining Q_{H-ads}, the ECSA is calculated as

$$\mathrm{ECSA_{Pt}}[\mathrm{m^2/g_{Pt}}] = \frac{Q_{H-ads}[\mathrm{C}]}{210\,\mu\mathrm{C/cm^2_{Pt}} \cdot 0.77 \cdot m_{Pt}[\mu\mathrm{g_{Pt}}]} \cdot 10^8 \tag{2.13}$$

where $210\,\mu\mathrm{C/cm^2_{Pt}}$ is the charge of full coverage for polycrystalline platinum and 0.77 is a factor to correct for not all catalyst being used [6]. The mass m_{Pt} is the mass of the catalyst loaded onto the electrode.

2.3.3 *iR* drop and compensation

The potential difference between the WE and RE in an electrochemical cell will not be equal to the voltage applied due to a loss of voltage caused by the solution between these electrodes. This voltage loss is equal to iR where R is the resistance of the solution. Because of this, the potential difference ΔE between the WE and the RE will be

$$\Delta E = \Delta V - iR \tag{2.14}$$

where ΔV is the voltage applied. The potential difference can thus be calculated by compensating for the iR term with a resistance R_u. One method that can be used to measure R_u is electrochemical impedance spectroscopy (EIS). At high frequencies, the impedance of the electrical double layer will be close to zero since it is a capacitance. Then, the only resistance will be that of the solution, R_u [19].

2.3.4 Rotating disk electrode

When evaluating electrocatalysts, the rotating disk electrode (RDE) method is commonly used. This is due to the method's simplicity and ability to give a meaningful prediction of the electrocatalyst's performance in an MEA [5]. The commercial availability of the components needed, like rotators and disks, at an acceptable cost is also a reason for the popularity of RDE [20]. RDE is performed in a three-electrode cell, and is a technique where the WE is a disk that is rotated around its vertical axis. The disk could be made from many different materials, for example glassy carbon (GC), and has a radius of 0.1 – 1.0 cm. It is surrounded by an insulating sheath with a significantly larger radius. Only one face of the disk is exposed to the electrolyte and the RDE pumps solution towards the disk through its rotation. Once the solution hits the solid electrode it is thrown outwards. With some theoretical work, a diffusion layer is defined where diffusion is the only mode of transportation. From this layer, one can derive the current density of the WE at potentials where the electrode reaction is mass control limited. The expression for this current density is the Levich equation [8]

$$j_d = 0.62nFD^{2/3}c\nu^{-1/6}\omega^{1/2} \tag{2.15}$$

where n is the number of electrons of the reaction, $F = 96\,485\,\mathrm{C/mol}$ is the Faraday constant, D is the diffusion constant, c is the concentration of the electroactive species dissolved in the electrolyte, ν is the kinetic viscosity of the electrolyte and ω is the rotation rate of the RDE with unit rad/s.

The limited diffusion layer and establishing of a high rate and steady-state mass transport makes the RDE method suitable for studying the kinetics of interfacial processes [17]. This includes the ORR activity of fuel cell catalysts, which is usually measured while the electrode is rotating at 1600 rpm [6]. When measuring the ORR activity, the electrolyte in the electrochemical cell needs to be saturated with O_2. Using 0.1 M $HClO_4$ saturated with O_2 as the electrolyte, the parameters $n = 4$, $D_{O_2} = 1.93 \times 10^{-5}\,\mathrm{cm^2/s}$, $c_{O_2} = 1.26 \times 10^{-3}\,\mathrm{mol/l}$, $\nu_{HClO_4} = 0.010\,09\,\mathrm{cm^2/s}$, and $\omega = 1600\,\mathrm{rpm}$ can be used in the Levich equation to achieve a theoretical current density of about $6\,\mathrm{mA/cm^2}$ [5]. When studying fuel cell catalysts with RDE, the catalyst is coated as a thin film on a GC disk, ideally $\leq 0.2\,\mu\mathrm{m}$ [6]. This is performed by preparing an ink containing catalyst and solvent and then letting it dry on the GC disk.

In the region 0.75 – 1.00 V vs. RHE of an ORR polarization curve, there is a steep slope as seen in Figure 2.4 which is the mixed kinetic-diffusion control region [6]. Below this there is flat region where the current is limited by the speed of diffusion, in range 0.20 – 0.70 V. As mentioned before, the current here should be about $6\,\mathrm{mA/cm^2}$. The quality of the coated thin film on the GC disk has a great impact on the ORR polarization curve. A good quality film should be uniform and cover the entire disk of the electrode. A worse coating leads to a less negative and more inconsistent current density in the region 0.80 – 1.00 V vs. RHE which means that it has a lower activity [21].

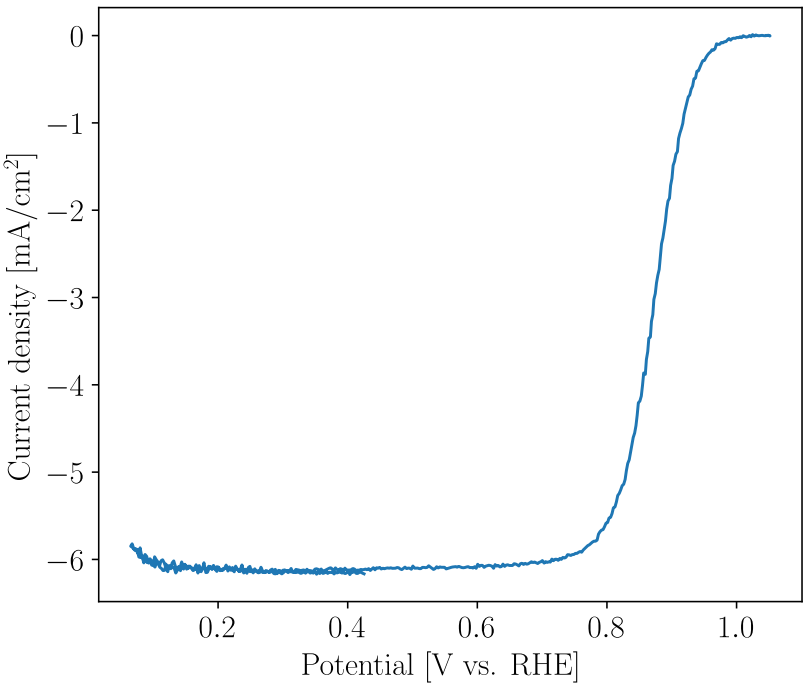

Figure 2.4: A typical voltammogram for an electrode coated with Pt/C catalyst in an O_2-saturated electrolyte.

The catalytic activity is usually determined by the current at 0.90 V vs. RHE. This potential is chosen in order to minimize the impact of mass-transport losses which can not be excluded at potentials lower than 0.90 V vs. RHE, where the current density is higher [6]. To correct for mass-transport losses, the Koutecky–Levich equation [5]

$$\frac{1}{i} = \frac{1}{i_k} + \frac{1}{i_d} \tag{2.16}$$

is used, where i_k is the kinetic current, i_d is the diffusion limited current and i is the current measured at 0.90 V vs. RHE [6]. The diffusion limited current is measured at 0.4 V vs. RHE or elsewhere in the flat region of Figure 2.4. Both i_d and i are background corrected. Background correction is done by performing the same CV measurement in a N_2-purged electrolyte. This current will be subtracted from the current measured with the O_2-saturated electrolyte to get a background corrected ORR current, eliminating current contributions from sources other than the ORR [6]. The Pt mass-specific activity (MA) is then estimated by dividing i_k with the mass of platinum loaded onto the WE:

$$\mathrm{MA} = \frac{i_k}{m_{Pt}}. \tag{2.17}$$

The Pt area-specific activity (SA) is calculated in a similar manner, i_k is divided by the ECSA and mass of platinum (or just the ECSA if it is not mass normalized) in the film:

$$\mathrm{SA} = \frac{i_k}{\mathrm{ECSA}_{\mathrm{Pt}} \cdot m_{Pt}}. \tag{2.18}$$

The current i_k is negative by convention, meaning that the MA and SA will be negative as well. In the results however, the MA and SA will be presented as their absolute value.

2.4 Other catalyst characterization methods

In addition to electrochemical techniques, many other methods exist that can be used for characterizing fuel cell catalysts. The size of Pt nanoparticles can be measured with both x-ray diffraction and transmission electron microscopy (TEM) [22]. As discussed by Mauyrhofer et al. larger nanoparticles, which have a lower specific surface area, require a higher platinum loading in RDE measurements in order to spread across the entire electrode disk [23]. TEM can also be used to display the morphology of the carbon support. The surface area of the carbon support can be measured with the Brunauer-Emmet-Teller (BET) method [22]. This method calculates the surface area from measurements of physical adsorption of a gas on a solid surface, usually utilizing nitrogen [24].

Zeta potential is a measure for the surface charge of nanoparticles and colloids and could be seen as a degree of electrostatic repulsion between particles [25]. For Pt/C catalysts, it could be related to agglomeration. Liu et al. [26] found that an increase of the ionic strength, by addition of NaCl, lead to a decreased zeta potential, an increased agglomerate growth rate and a worse stability. Both zeta potential and

agglomerate size in an ink used for RDE was found to be related to the pH of said catalyst ink by Inaba et al. [27]. A larger pH resulted in a zeta potential of larger magnitude and smaller agglomerates and they found that this had a positive effect on the stability of the ink, as well as the measured SA. Inaba et al. used electrophoretic light scattering and dynamic light scattering to measure the zeta potential and agglomerate size, respectively.

Khandavalli et al. [28] measured the rheology of two different carbon supports, with and without platinum. When adding ionomer to a catalyst ink, the viscosity decreased and the two supports had a minimum viscosity at different ionomer/carbon weight ratios (I/C). A decreased viscosity indicates a decrease in the size of the agglomerates, which was verified with ultra-small-angle x-ray scattering. This indicates that ionomer stabilizes carbon agglomerates and that different carbon supports have different optimal I/C ratios [28].

3

Methods

To measure the ORR activity of a catalyst, some preparation is needed. First, an ink must be prepared my mixing the catalyst with a solvent. A few microlitres of the ink is then deposited onto the GC disk of the electrode where it is dryed. Lastly, the ECSA and ORR activity can be measured with the electrode in an electrochemical cell.

3.1 Ink preparation

Two different commercial Pt/C catalysts were used, Catalyst A and B. Both catalyst have a metal content of about 50 wt% and they have a particle size of 5.1 – 5.7 nm and 3.4 – 4.9 nm respectively. The support material for catalyst A is high surface area carbon with a surface area of 780 m^2/g and catalyst B has a durable high surface area carbon support with a surface area of 800 m^2/g.

Several inks were prepared in order to study the ink recipe's effect on the quality of the coating. For each ink, a cleaned 20 ml glass vial was used. The vial was placed on a precision balance (OHAUS Explorer^{TM}) where the catalyst is added. The balance's ionizer was used before and after adding the catalyst to remove static charges. Ultrapure (UP) water from a PURELAB Chorus 1 with a purity of 18.2 MΩcm was then added, before other solvents to prevent spontaneous combustion of the catalyst when adding alcohol. After this, 2-Propanol AnalaR NORMAPUR® Reag. Ph. Eur., Reag. USP, ACS, VWR (IPA) was added and the lid of the vial was closed to hinder evaporation. Lastly, an ionomer, Nafion^{TM} PFSA 5 wt% Dispersion D520CS, was added as part of a solution where it had been further dispersed to 1 wt% with UP water for the purpose of making it easier to work with by lowering the viscosity. For each ink, the aim for the ionomer/carbon weight ratio (I/C) was 0.25 – 1.0. The aim for the water:alcohol ratio and the Pt loading were varied in order to study their effect on the quality of the coating. For catalyst A, inks with alcohol contents of about 10, 19 and 21.5 vol% alcohol and a Pt loading of about 20.0 µg/cm^2 were prepared. Two additional recipes for 19 vol% alcohol were prepared with Pt loadings of 10.0 and 35.0 µg/cm^2. Two inks were made per recipe, as well as an extra ink with 24.0 vol% alcohol and Pt loading 20.0 µg/cm^2. The recipes of all inks made are shown in Table 3.1.

For catalyst B, the aim for the Pt loading was 20.0 µg/cm^2 for all inks and only one inks was made per recipe. Inks were made with 10, 19, 22 and 25 vol% alcohol.

The intention for the ink with 25 vol% was to put a smaller volume of ink on the WE in order to reduce the risk of the ink spreading outside of the GC disk. Thus, the catalyst content per volume was increased in order to keep the Pt loading at 20 µg/cm^2. Two additional inks with 22 vol% were prepared, inks 16 and 17 in Table 3.1. After dispersion of the inks, a few microlitres of 0.2 or 1.0 M KOH (Honeywell Fluka^{TM}) were added successively to increase the pH, measuring the pH with a Metrohm 913 pH meter after each addition of KOH. In total, about 19 µl of 0.2 M KOH was added to ink 16 which increased the pH from 4.1 to 6.1. For ink 17, 50 µl of 0.2 M KOH increased the pH from 4.1 to 7.5 and 3 µl of 1.0 M KOH was then added, which further increased the pH to 9.5. Inks 18 and 19 were made to investigate the influence of KOH on the catalytic activity. 7 µl of 1.0 M KOH was added to ink 18 and the measured pH of ink 18 and 19 were 8.0 and 4.2, respectively.

Table 3.1: The ionomer/carbon weight ratio, alcohol content and Pt loading of every ink made for this study. The Pt loading assumes that 10 µl of ink dries on a 5 mm diameter disk except for ink 15 which assumes 7 µl of ink. KOH was added to ink 16 and 17, which then had a measured pH of 6.1 and 9.5, respectively.

Ink	**Catalyst**	**I/C**	**Alcohol [vol%]**	**Pt loading [µg/cm^2]**
1	A	0.41	11.2	19.5
2	A	0.40	11.1	19.5
3	A	0.40	19.1	19.9
4	A	0.38	19.3	19.9
5	A	0.48	21.4	19.6
6	A	0.45	21.5	19.8
7	A	0.40	24.4	19.6
8	A	0.42	19.5	34.8
9	A	0.41	19.5	34.8
10	A	0.44	19.3	10.0
11	A	0.43	19.2	10.0
12	B	0.36	11.1	19.5
13	B	0.45	19.4	19.8
14	B	0.44	22.0	19.8
15	B	0.43	25.1	19.5
16	B	0.44	21.8	19.8
17	B	0.43	21.4	19.8
18	B	0.42	21.3	20.0
19	B	0.39	21.3	19.9

After mixing catalyst, UP water, 2-propanol and ionomer, the inks were dispersed using a Hielsher UP400St ultrasonic disperser with a 3 mm sonotrode (S24d3). During the dispersion, the vial is placed in cold water to avoid an increase in temperature. The energy input of the dispersion was 6200 Ws with an amplitude of 50 % for all inks.

3.2 Working electrode preparation

The WE used for the RDE measurements consists of a glassy carbon (GC) disk with a diameter of 0.5 cm in a polyether ether ketone (PEEK) tip as seen in Figure 3.1a. The GC disk first needs to be polished. This is done by using a polishing cloth, Al_2O_3 and UP water. A small amount of Al_2O_3 was added to the polishing cloth which was then wetted with UP water before mixing it with a pipette tip to form a slurry. The electrode is then polished by making a figure eight on the slurry and polishing cloth, ten times in both a clockwise and anti-clockwise direction. Afterwards, the WE is rinsed with UP water and wiped with acetone and a lint-free tissue. To check if the GC disk is clean, it is put under a Leica DVM6 microscope where it should look like Figure 3.1b. The microscope is used with an FOV 12.55 objective and the exposure, gain, ring light (RL) and coaxial light (CX) set to 18.5 ms, 1.00, 60 and 50, respectively. In case the electrode is not clean, the step of wiping with acetone and lint-free tissue is repeated until the electrode is clean.

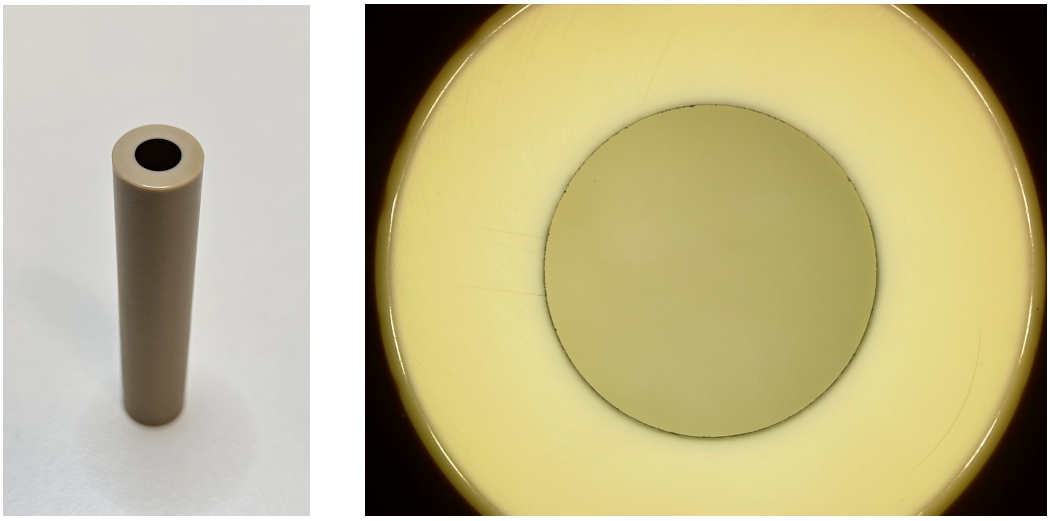

(a) The working electrode.

(b) A clean GC disk, surrounded by an insulating material, as seen in a microscope.

Figure 3.1: A clean working electrode and a microscope image of it from above.

Once the WE is polished, it and the tip of a micropipette is treated with an OHAUS static ionizer, ION-100A, to remove possible static charges to make the coating process easier. A 10 µl aliquot of ink is then deposited with a micropipette onto the 0.5 cm GC disk. If the ink spreads outside of the GC disk, it is cleaned up with a lint-free tissue and the electrode is once again cleaned with acetone. With 10 µl of ink successfully deposited onto the GC disk, the ink is dried while the electrode is spinning at 700 rpm and a small flow of N_2 is directed at the ink at an angle. The rotation and flow of N_2 is controlled with an in-house build device.

Once the ink is dried, it is inspected under a microscope with the same setup as when the cleanliness of the WE was checked. The coating is also studied with RL and CX set to 100 and 60 respectively and 50 and 80 respectively. These extra settings help with evaluating the coating and distinguish between homogeneous and

inhomogeneous coatings. Aside from the homogeneity and uniformity, the microscope is also used to make sure that the ink covers most of the GC disk and that it has not spread outside of the GC disk.

3.3 Electrochemical measurements

The measurements for the ECSA, SA and MA of the catalysts were performed in electrochemical cells. An RHE was used as the RE, specifically a Gaskatel Mini-Hydroflex, and a platinum sheet electrode (Metrohm) was used as the CE. An assembled setup is shown in Figure 3.2. The WE is mounted on the RDE rotator (Metrohm) which is connected with red and green banana connectors to a potentiostat (Metrohm). The CE and RE are connected with black and blue banana connectors respectively. Gas is supplied through the red tubes in Figure 3.2, one cell receives N_2 and the other receives O_2. The WE and CE are then moved between the cells, depending on what environment the measurement protocol requires.

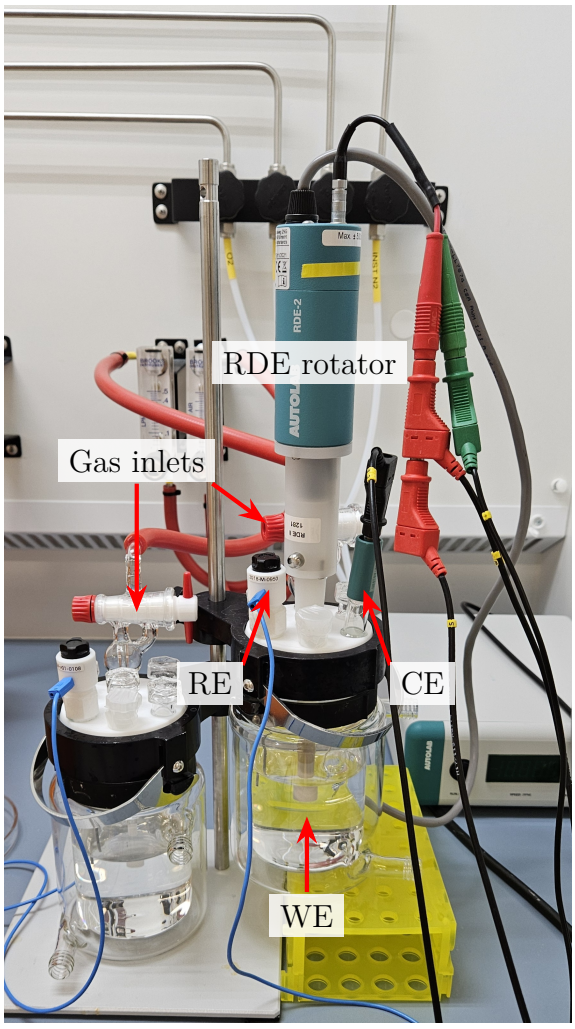

Figure 3.2: The RDE setup. Two cells, one completely assembled to the right and one missing the working and counter electrodes to the left.

3.3.1 Cleaning of the electrochemical cell

Before doing any measurements, the glassware used must be thoroughly cleaned. The cell vessel and its accessories are first cleaned with normal dish soap. The cell vessel is then filled with, and its accessories soaked in, 1 vol% Mucasol (Schülke) in UP water for at least 30 min. The cell vessel is then rinsed eight times with UP water. The lid and its o-ring and the gas inlets are rinsed for 60 s and the rest of the accessories are rinsed for 30 s with UP water. After rinsing the cell vessel, it is filled with 95 % sulphuric acid (VWR) to stand over night. The next day the cell is rinsed eight times with UP water again. It is then rinsed three times with the electrolyte to remove any trace of UP water before being filled with 200 ml of electrolyte. Lastly, the cell is assembled with lid, gas inlets and plugs as seen in Figure 3.2. The electrolyte used is 0.1 M $HClO_4$ from Fisher Chemical. Two cells were prepared for each measurement, one saturated with N_2 and one with O_2. Bubbling with the respective gases for the two cells was performed for at least 30 min with a flow of 0.1 l/min. Cleaning of the O_2 saturated cell was done every measurement day and the N_2 saturated cell was cleaned every third measurement day.

3.3.2 Measurements of the electrochemical surface area

Before measuring the ORR activity, the ECSA of the coating is measured. The electrode is mounted on an RDE rotator and submerged into the electrolyte saturated with N_2. In the case of air bubbles on the coating, these are removed by turning on the RDE rotator to 2000 – 3000 rpm and dipping the tip of the electrode up and down into the electrolyte. The WE, RE and CE are all connected to a potentiostat. First, the sample is pre-treated by sweeping the potential over the range 0.04 – 1.2 V vs. RHE for 60 cycles with the scan rate 100 mV/s. Then the potential is swept over the same range once again but with a slower scan rate, 20 mV/s. This measurement is used to calculate the ECSA, as explained in Section 2.3.2. The CV curve is integrated over the hydrogen adsorption region, the marked area in Figure 2.3 and the integrated charge is then used in Equation 2.13 to calculate the ECSA. This equation also needs the mass of platinum m_{Pt}, which is calculated based on the amount of catalyst in the ink and the amount of ink deposited onto the GC disk.

3.3.3 Measurements of the oxygen reduction reaction activity

After measuring the ECSA, the same cell with N_2 saturated electrolyte is used to perform a background measurement. This is done by sweeping the potential between 0.04 and 1.05 V vs. RHE at a speed of 5 mV/s for two scans. The WE and CE are then moved to another cell which contains electrolyte saturated with O_2 and its own RE. The WE, CE and RE are all connected to a potentiostat again and the potential is swept over the same range and at the same speed as the background measurement for two scans. For this measurement, the rotation of the RDE rotator is turned on to rotate at 1600 rpm, a speed commonly used in literature [5, 6, 20].

An electrochemical impedance spectroscopy (EIS) measurement is also done in the

O_2 saturated electrolyte. This is done at 0.7 V vs. RHE in the frequency range 100 kHz to 1 Hz. The resistance measured when the imaginary part of the impedance is zero is the resistance of the solution. This measured resistance is used to compensate for the iR drop in the measured potential in the background and ORR measurements.

After compensating for the iR drop, the current from the background measurement is subtracted from the ORR measurement to obtain a background corrected current. The background corrected currents at 0.4 and 0.9 V in the first scan in the positive direction are used in Equation 2.16 to obtain the kinetic current. Dividing this current by m_{Pt} or the (not mass normalized) ECSA yields the MA and SA, respectively.

4

Results and discussion

This chapter presents and discusses the results of the experiments performed. The discussion highlights the influence of alcohol content, as well as platinum loading, on the quality of coatings for RDE measurements and the results of said measurements for catalyst A. For catalyst B, the discussion instead focuses more on the stability of the ink and if this could be improved by adjusting the pH of the catalyst ink.

4.1 Alcohol content

The influence of the water:alcohol ratio of the ink on the coating quality was investigated for both catalysts. For catalyst A, this included testing three ratios, both visually with microscopy and electrochemically with RDE. Two inks were made per recipe in case there were errors or other sensitive parameters during the ink formation. For catalyst B, four water:alcohol ratios were tested but it proved difficult to achieve a uniform coating with any of them. Thus, most of the time for this catalyst was spent varying different parameters during ink formulation and not verifying the results with multiple inks per recipe. Only one ink was therefore made for each of the water:alcohol ratios tested with catalyst B. Furthermore, no RDE measurements were performed to test how the water:alcohol ratio affects the ORR activity for these inks.

An alcohol content of 11 vol% was used as a starting point since about 10 vol% IPA has been commonly used at PowerCell Group AB previously. Most literature however use a higher alcohol content, 24 or 25 vol% [6, 20, 27, 29] and thus, the difference between a lower and a higher water:ratio was investigated.

4.1.1 Coating qualities

Inks with a higher alcohol content tended to spread out more on the GC disk, likely due to the lower surface tension of IPA compared to water [29]. This made it easier for these inks to cover (close to) the entire GC disk, but also made it easier to spread outside of the disk, making the coating process more difficult. This is shown in Figure 4.1 where Figure 4.1a has 11 vol% IPA and does not cover the entire disk as opposed to Figure 4.1b with 21.5 vol% IPA. In Table 3.1, these are inks 1 and 5, respectively. No noticable difference was observed between inks with 19 and 21.5 vol% IPA. For ink 7 in Table 3.1, with 24.4 vol% IPA, it was not possible

to produce a coating since the ink would always spread outside of the GC disk. Therefore, the surface tension seems to be too low for depositing a total of 10 µl on a GC disk with a 5 mm diameter.

Most studies use and recommend an alcohol content of 24 or 25 vol% for 50 % Pt/C catalysts [6, 20, 27, 29]. A reason for why this seems to be too high for ink 7 could be that different catalysts behave differently, and work best with different water:alcohol ratios [30]. The quality of the electrode could be another reason, perhaps influenced by how it is cleaned. Interactions between the ink and the GC and GC/PEEK border decide how the ink droplet behaves on the electrode. Thus, maybe individual GC disks influence the ink dynamics differently.

Some coatings contain spots of lighter color, implying less catalyst, as seen in Figure 4.1d. After some investigation of the inks and the coating procedure, these spots are most likely a result of a too large flow of N_2 during the drying process. An even higher flow of N_2 seems to result in spots of no catalyst where the GC can be seen, as shown in Figure 4.1e. Figure 4.1c on the other hand, shows that a too small flow results in an inhomogeneous coating with a slightly brighter color, encircled by a darker ring. From these observations, a coating such as Figure 4.1b seems to require the flow rate of N_2 to be optimized such that it hits the ink but doesn't blow it away, a rate that could differ depending on the angle and height of the flow.

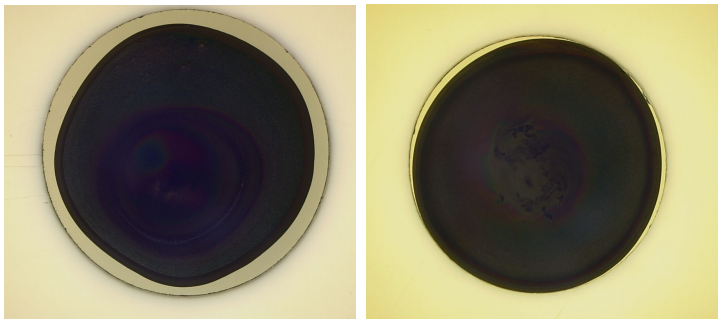

(a) Does not cover the entire GC disk

(b) Covers most of the GC disk

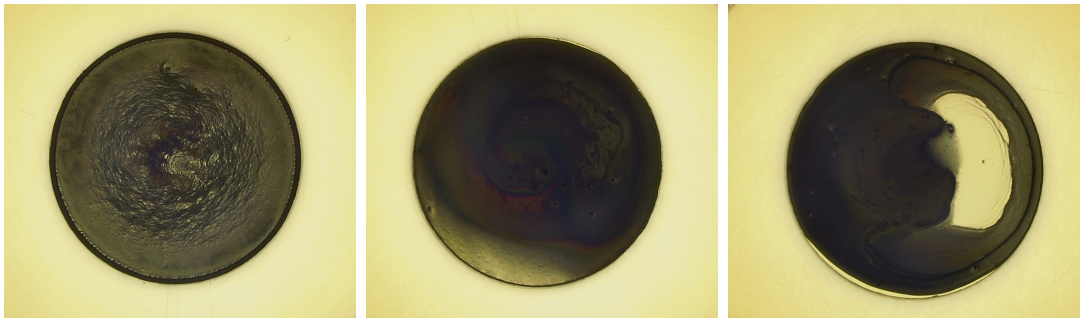

(c) Too low flow of N_2

(d) Slightly too high flow of N_2

(e) Too high flow of N_2

Figure 4.1: A few different coatings which depict how inks cover the GC disk differently depending on alcohol content ((a) with 11 vol% IPA and (b) with 21.5 vol% IPA) and the influence of the N_2-flow during drying ((c) – (e)).

Coating an electrode can be difficult and the homogeneity could depend on the operator's skill. Therefore, some studies have tried to automate this procedure. For example, Ke et al. [31] used a device that transfer droplets in the size of $\sim 3\,\mathrm{nl}$ onto a GC disk with a precision of $\sim 1\,\mu\mathrm{m}$. Another approach was used by Inaba et al. [32] who sprayed the ink onto the GC disk with an ultrasonic atomizer. The GC and holder were separable in this case such that the holder could be changed or cleaned after spraying. However, a major disadvantage with this technique is that the amount of catalyst that is deposited onto the GC disk is unknown and must be estimated from ECSA measurements.

4.1.2 Activity results

The average currents at 0.9 V vs. RHE and mass limited currents of each tested water:alcohol ratio for catalyst A are shown in Figure 4.2. These currents are used to calculate the kinetic current with equation 2.16 which in turn is used to calculate both the MA and SA. Figure 4.3 shows the average ECSA, MA and SA for the same samples as Figure 4.2.

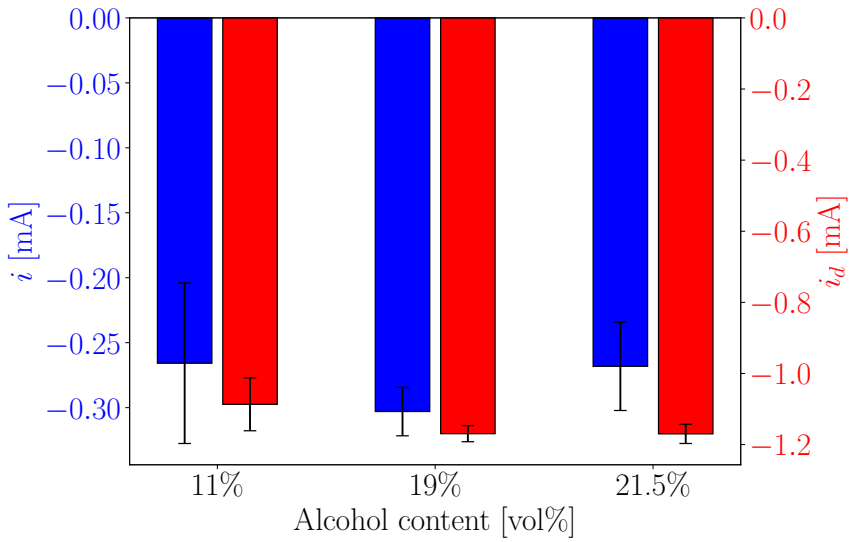

Figure 4.2: The average current at 0.9 V vs. RHE i and diffusion limited current i_d for inks with different alcohol contents. The error bars show the standard deviation of the data points used for each mean value.

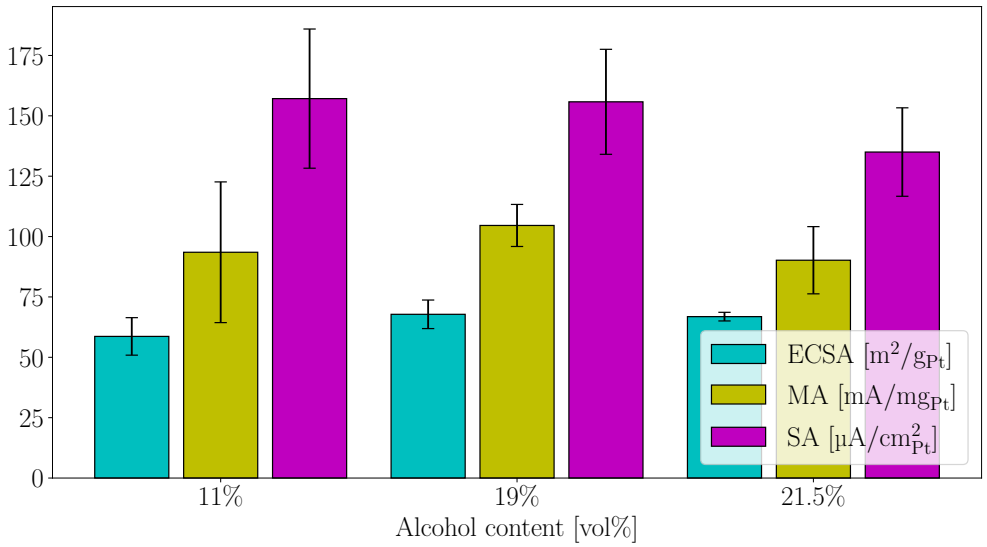

Figure 4.3: The average ECSA, MA and SA for inks with different alcohol contents. The error bars show the standard deviation of the data points used for each mean value.

Comparing the diffusion limited currents, they are about the same for most coatings. The exception is one of the inks (ink 1 in Table 3.1) with 11 vol% IPA where the coatings covered a smaller portion of the GC disk, probably leading to a less negative diffusion limited current. According to the Levich equation, the diffusion limited current density should be about 6 mA/cm^2. A current density of 6 mA/cm^2 equals a current of about 1.18 mA for a disk with diameter 5 mm. If the area which the coating covers then is smaller, it makes sense for the current to be smaller, given that the current density is the same.

Ink 1 also has a lower MA and ECSA, probably due to an error in the weighing of catalyst since its SA is still comparable to the other ink with 11 vol% IPA and the inks with 19 vol% IPA. The ECSA should not be as sensitive as the MA and SA to the quality of the film [33]. Therefore, it is thought that the measured ECSA should not vary too much for different coatings. However, the other ink with 11 vol% IPA also has a lower ECSA than the inks with higher IPA content, even if the difference is much smaller compared to ink 1.

In Figure 4.3, 21.5 vol% IPA has the lowest average activity due to one of the inks with this recipe having a lower activity. For the other ink with 21.5 vol% IPA, the activity os similar to the coatings made from inks with 19 vol% IPA. The parameters of these two inks with 21.5 vol% IPA are almost identical and a few more inks would be needed to say if the difference in activity is due to some error in the ink preparation or if this recipe is sensitive to small variations in its parameters. The errorbars in Figure 4.3 does overlap with each other which could mean that this is simply caused by uncertain measurements.

Takahashi et al. explored the influence of IPA content on the ECSA to quantify

how well dispersed an ink is, and found that the ECSA peaked at 35 vol%. For a Pt/C catalyst that is not heat treated, this peak is rather shallow [30] and their results are similar to the measured ECSA in Figure 4.3. In Figure 4.3, the lower alcohol content produced a lower ECSA even if there might be some overlap of the errorbars, and 19 vol% and 21.5 vol% have similar ECSAs, like the shallow peak shown by Takahashi et al. where small variations in IPA content does not affect the ECSA significantly. They link the ease of forming a good dispersion and being less sensitive to IPA content to the catalyst not being very hydrophobic [30]. The similar results in ECSA, SA and MA in Figure 4.3 is therefore most likely due to catalyst A not being particularly hydrophobic. This would mean that it is not too sensitive to the alcohol content and fairly easy to achieve a good dispersion, behaviours that has been observed.

4.1.3 Ink stability and coating qualities for catalyst B

Ink stability was not an issue for catalyst A, with the possibility of making adequate coatings at least a week after ink preparation. The same cannot be said for catalyst B. The coatings made with catalyst B are hard to compare since none of the inks prepared with different water:alcohol ratios seem to be stable over time. With 11 vol% IPA, the coating seems to contract and cover a much smaller area of the GC disk than the ink covered before drying. However, this coating was done several days after the ink preparation, and similar behaviour was observed from ink with higher alcohol contents already two days after ink preparation as shown in Figure 4.4d-f. The coatings with 22.0 vol% IPA, which were made the same day as the ink seem to be the best, but are still not homogeneous. None of the coatings with 19.4 or 25.1 vol% were better than those, but these were made one day after ink preparation which could explain their worse quality. Additionally, for the ink with 25.1 vol% IPA, the catalyst concentration was increased in order to keep the same Pt loading with a smaller aliquot of ink on the GC disk (Figure 4.4c and f). Increasing the ink's concentration of catalyst in this way could possibly affect the coating quality or have other unseen effects, but this has not been investigated further.

Compared to catalyst A, catalyst B is heat treated, something which could increase its hydrophobicity which in turn makes it difficult to achieve a good coating [30]. Takahashi et al. found that a heat treated catalyst had a sharper and more distinct peak in ECSA vs. IPA content compared to a standard Pt/C catalyst. The peak would indicate at which alcohol content the ink has the best dispersion and was found at 35 vol% [30], higher than what was tested for this thesis. An ink with that high alcohol content would most likely be too difficult to deposit 10 µl of on the GC disk without the ink spreading outside of the disk. Decreasing the volume and increasing catalyst concentration like with Figure 4.4c could be an option. 25 vol% IPA does not seem to be much of an improvement compared to 19 vol% in Figure 4.4a and c, but maybe an even higher IPA content could be better.

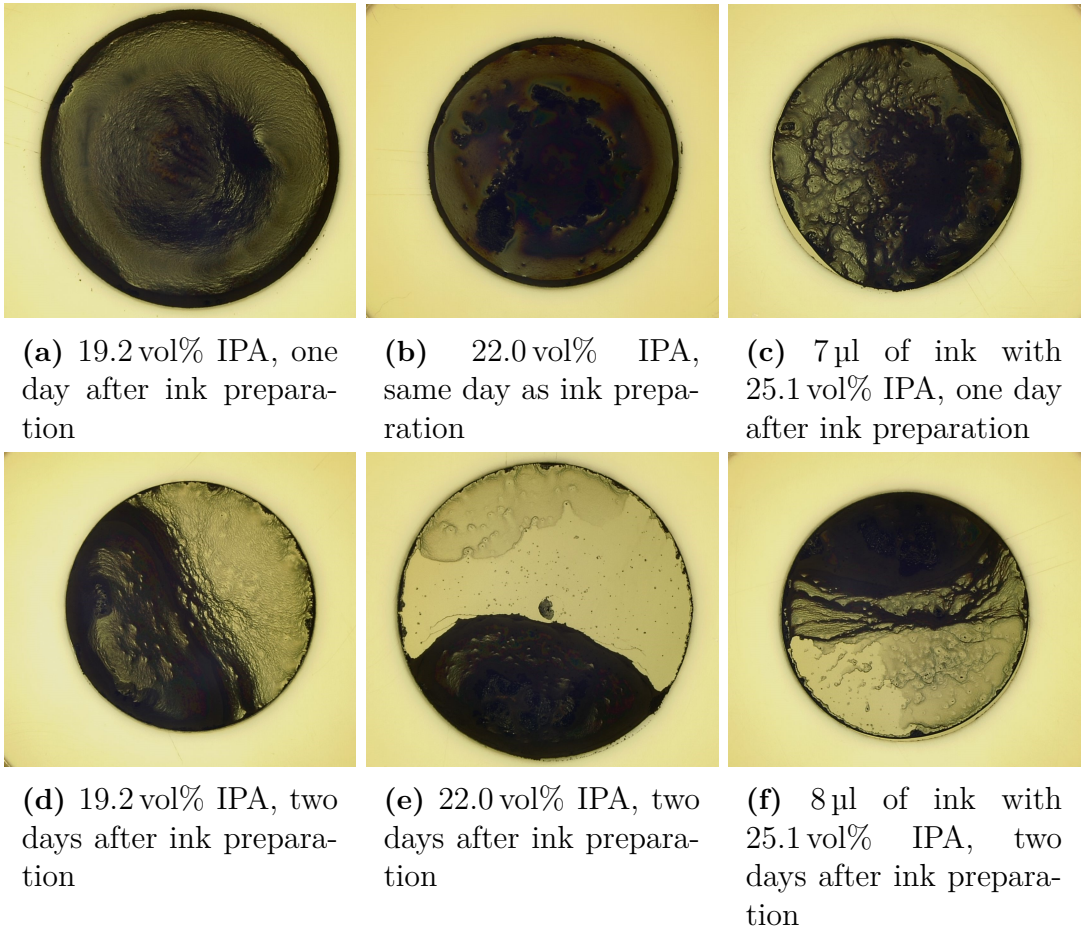

(a) 19.2 vol% IPA, one day after ink preparation

(b) 22.0 vol% IPA, same day as ink preparation

(c) 7 µl of ink with 25.1 vol% IPA, one day after ink preparation

(d) 19.2 vol% IPA, two days after ink preparation

(e) 22.0 vol% IPA, two days after ink preparation

(f) 8 µl of ink with 25.1 vol% IPA, two days after ink preparation

Figure 4.4: A few different coatings with three different inks containing catalyst B.

4.2 Platinum loading

Three different Pt loadings were tested with catalyst A, shown as inks 3, 4, 8, 9, 10 and 11 in Table 3.1. These loadings are about 10, 20 and 35 $\mu g_{Pt}/cm^2$ and this section studies how this parameter influences the coating quality and ORR activity.

4.2.1 Coating qualities

Figure 4.5 shows coatings with high and low Pt loadings, 34.8 $\mu g/cm^2$ and 10.0 $\mu g/cm^2$, respectively. A high Pt loading yields a homogeneous film, similar to those with 20 $\mu g/cm^2$ Pt loading. A lower Pt loading on the other hand, 10 $\mu g_{Pt}/cm^2$, yields more inhomogeneous films. The lighter regions that are causing this inhomogeneity is probably regions with less catalyst. Therefore, such a low Pt loading does not seem to contain enough catalyst for the Pt to cover the GC disk uniformly.

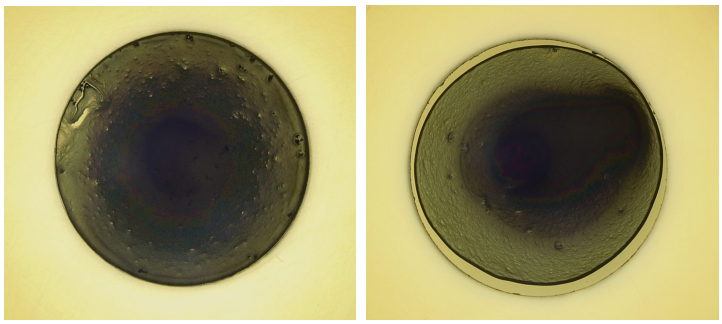

(a) First ink with Pt loading 10.0 µg/cm^2

(b) Second ink with Pt loading 10.0 µg/cm^2

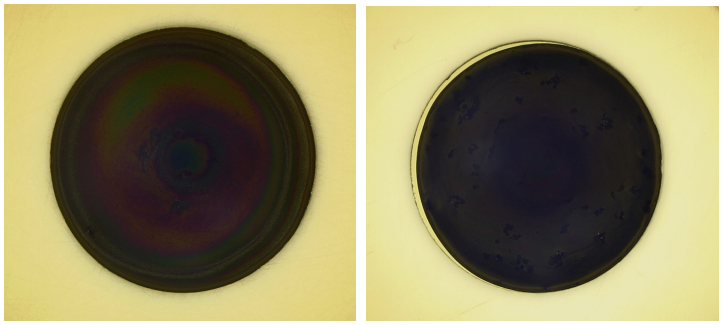

(c) An ink with Pt loading 19.9 µg/cm^2

(d) An ink with Pt loading 34.8 µg/cm^2

Figure 4.5: Coatings made from inks with low and high Pt loadings. Both inks for the low Pt loading are displayed to highlight the difference between the coatings.

4.2.2 Activity results

A low Pt loading has a less negative diffusion limited current as seen in Figure 4.6. This is probably related to the catalyst not covering the GC uniformly as shown in Figure 4.5. One of the inks with low Pt loading also have a very high ECSA and MA, but the SA is similar to the other inks. There might an error in the weighing of catalyst here. Comparing the coating qualities with a microscope, this is further strengthened by Figure 4.5a being less bright around the edges and having a more homogeneous coating than Figure 4.5b, with both having a supposed Pt loading of 10 µg$_{Pt}$/cm^2. This difference in appearance is most likely caused by a higher Pt loading for the coating in Figure 4.5a. Comparing the ECSAs in Figure 4.7, the Pt loading of this ink should be about 16.1 µg$_{Pt}$/cm^2 for the ECSA to be similar to the other inks with catalyst A. Comparing the Pt loadings 19.9 and 34.8 µg$_{Pt}$/cm^2, the MA and SA are very similar and the difference between their mean values is less than the variation in their respective data sets. The lower SA for coatings with Pt loading 10 µg$_{Pt}$/cm^2 could be caused by their inhomogeneity causing uncertain measurements. Additionally, the errorbars for SA does overlap in Figure 4.7 meaning that the difference in SA is not too large between 10, 19.9 and 34.8 µg$_{Pt}$/cm^2.

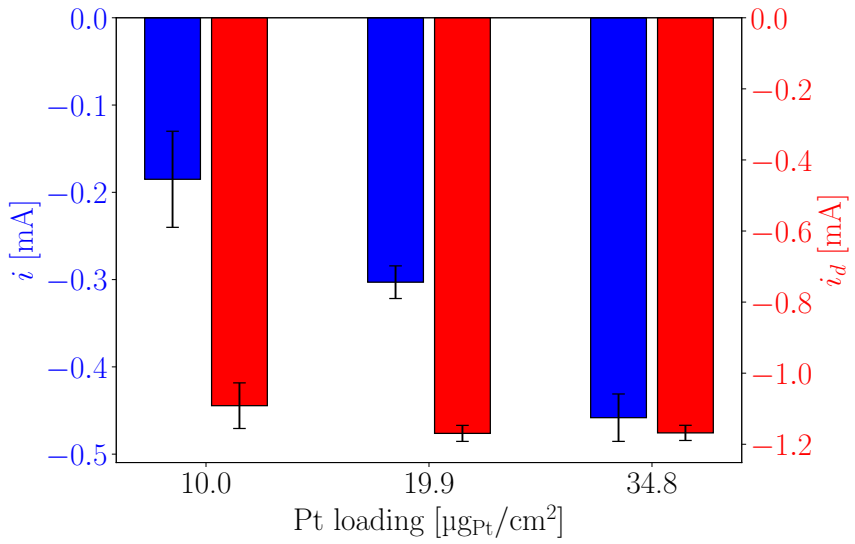

Figure 4.6: The average current at 0.9 V vs. RHE and diffusion limited current for inks with different Pt loadings. The error bars show the standard deviation of the data points used for each mean value.

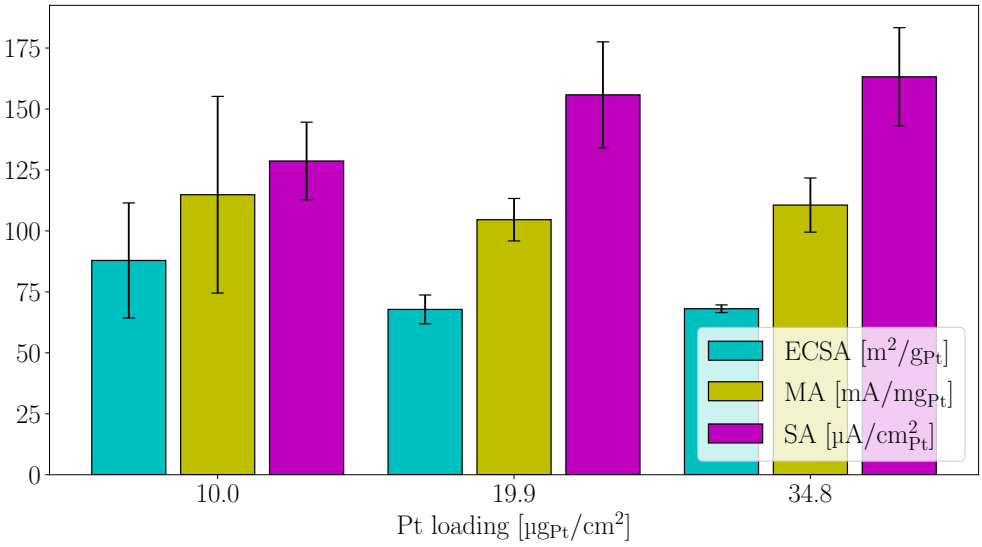

Figure 4.7: The average ECSA, MA and SA for inks with different Pt loadings. The error bars show the standard deviation of the data points used for each mean value.

A lower diffusion limited current as a result of a low Pt loading is shown by Mayrhofer et al. as well, with the explanation that the catalyst is not able to spread across the entire GC disk [23]. Catalysts tested by Mayrhofer et al. with a surface area of 60 m^2/g experienced this at a Pt loading of 3.5 $\mu g_{Pt}/cm^2$. This Pt loading is

even lower than what was shown to be too low for catalyst A in Figure 4.6, but the optimal Pt loading most likely depends on what catalyst is used. For too high platinum loadings, Mayrhofer et al. argues that a too thick film changes the RDE mass characteristics. The SA will then be influenced by unknown parameters such as agglomerate structure, particle contact and diffusion of oxygen in the ionomer. The kinetic region of the ORR curve will also shrink and become steeper due to a very high activity causing the current to quickly become diffusion limited [23]. Seeing how the activities of $34.8\,\mu g_{Pt}/cm^2$ and $19.9\,\mu g_{Pt}/cm^2$ are similar in Figure 4.7, the limit of how high the Pt loading can be for catalyst A does not seem to be reached at $34.8\,\mu g_{Pt}/cm^2$.

4.3 Influence of pH on coating quality

As mentioned in section 4.1.3, inks with catalyst B seems to suffer from stability issues, with the quality of coatings dropping with time since ink preparation. Because of this, the effect of the pH of an ink on the coating quality was investigated as this might help increase its stability [27]. KOH was added to inks 16 and 17 in Table 3.1, with the recipe otherwise being the same as the ink used in Figure 4.4b, ink 14 in Table 3.1. Without adding KOH, the pH of inks 16 and 17 were both about 4.1. After adding 19 µl of 0.2 M KOH to ink 16, the pH increased to 6.1. For ink 17, 50 µl of 0.2 M KOH was added which increased the pH to 7.6. After an additional 3 µl of 1.0 M KOH was added, the pH increased to 9.6.

Comparing the coatings with KOH to those without, those with KOH seem similar to the coatings made with ink 14 the same day as the ink preparation (Figure 4.4b), and retains this appearance at least two days after inks preparation as shown in Figure 4.8. This seems to indicate that adding KOH increases the stability of the ink. At pH 9.6, the coating looks worse than for those with pH 6.1 and 7.5, perhaps indicating that the pH was increased too much.

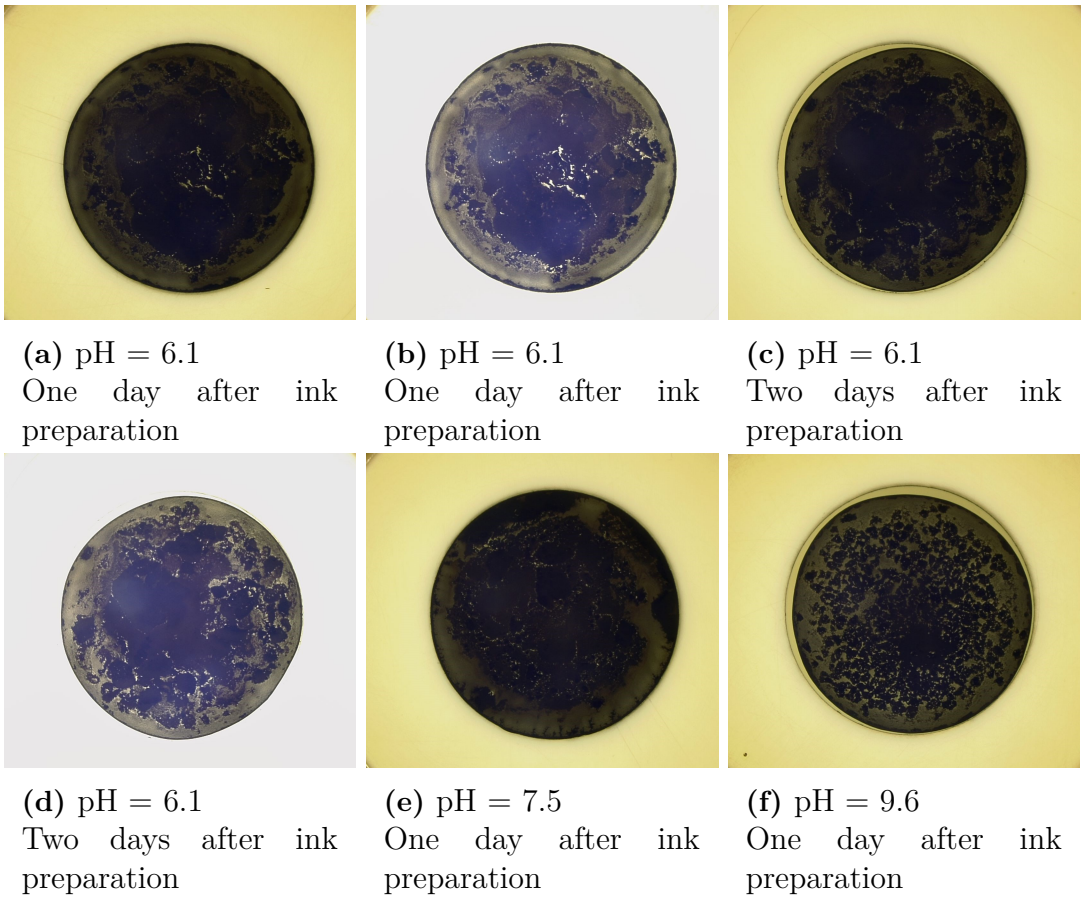

(a) pH = 6.1
One day after ink preparation

(b) pH = 6.1
One day after ink preparation

(c) pH = 6.1
Two days after ink preparation

(d) pH = 6.1
Two days after ink preparation

(e) pH = 7.5
One day after ink preparation

(f) pH = 9.6
One day after ink preparation

Figure 4.8: Coatings for catalyst B where KOH has been added to the ink. For pH of 6.1, a microscope picture with a brighter coaxial light is supplied ((b) and (d)).

The effect of KOH on the activity was studied by performing RDE measurements on two coatings made from an ink with KOH (ink 18), and two coatings made from an ink without (ink 19). The pH was measured to be 8.0 and 4.2 for the inks with and without KOH, respectively. All of these four coatings were made one day after ink preparation and the ink with KOH yielded coatings of better quality, similar to what has previously been discussed with Figure 4.4 and 4.8. Table 4.1 displays the results of the RDE measurements done on the coatings. Both the ECSA and ORR activity of ink 18 is slightly higher than for ink 19, but the difference is minimal when compared to the results of catalyst A. This increase seems to indicate that the addition of KOH increases the activity but it is unclear whether this increase is only attributed to the improved visual quality or if the KOH has any other unseen influence. Experiments with other techniques would be needed to get a better understanding of why KOH improves the activity. It is also not certain that this increase would still be present if more measurements would be performed due to the increase being so small.

Table 4.1: The results of RDE measurements performed on two coatings with KOH, and two without.

Ink	pH	ECSA [m^2/g]	i [mA]	i_d [mA]	MA [mA/mg_{Pt}]	SA [$\mu A/cm^2_{Pt}$]
18	8.0	70	−0.267	−1.19	88	126
18	8.0	65	−0.254	−1.18	83	128
19	4.2	60	−0.229	−1.12	73	121
19	4.2	61	−0.235	−1.13	76	125

As previously mentioned in section 2.4, Inaba et al. have studied how the pH of the catalyst inks affect the ORR activity [27]. They used two home-made and one commercial Pt catalyst with different carbon black supports. By adding 1 M KOH or 0.1 M $HClO_4$ to influence the pH, they found that an ink with higher pH had a much higher SA, but similar ECSA compared to one with a lower pH. For all catalysts, the SA was at least twice as high for an ink with a pH of 8, compared to a pH of 4 [27]. The effect of a higher pH is much smaller in Table 4.1 where the difference in SA is existent but minimal. It is unclear for how long the ink was aged before film fabrication in the case of Inaba et al. and maybe the results in Table 4.1 would differ more if an ink older than one day had been used due to differences in stability. One clear difference between these results and those of Inaba et al. however, is the drying method used for film fabrication. They used a technique where the ink does not include any ionomer, and the ink dries stationary on the electrode in a sealed beaker filled with IPA. This method, the one used in this report and two other similar methods were tested by Shinozaki et al. According to Shinozaki et al. the method used by Inaba et al. yields the thinnest and most uniform films as well as the highest ORR activity. However, it is a more sensitive technique compared to the method used in this thesis [29]. The difference in drying method or catalyst used could be the reason why SA vs. pH differs between Inaba et al. and Table 4.1. However, the results that pH increases stability agree with the findings of Inaba et al. [27]. Using dynamic light scattering and measuring the zeta potential, Inaba et al. concluded that a higher pH increases the surface charge of the catalyst, thus increasing the repulsion between the particles, resulting in a greater stability and hindering agglomeration [27]. This could explain the results shown in this report as well, with agglomeration being the cause for why the coatings seems to contract after a few days like in Figures 4.4d, e and f. Less agglomeration could also be the reason for why the ORR activity seems to increase with pH in Table 4.1.

4.4 Error analysis

Comparing the activity to microscope images of the coatings, a more homogenous coating usually corresponds to a higher activity. However this is not always the case, such as one of the inks with 21.5 vol% IPA. The three coatings, in order of least to most homogenous has an MA of 77, 91 and 77 mA/mg_{Pt}. It is worth noting that the current at 0.9 V is very sensitive to small changes in the potential. As mentioned

in the previous chapter, two REs were used. The difference in potential of these two electrodes was measured to be about 2 mV. For the first half of measurements, it is uncertain if the same RE was used for the ORR measurement every week, or if the REs were switched when both cells were cleaned at the same time. Even if the difference in potential is small, its impact on the current could be notable. A similar issue lies in that the current is measured at discrete potentials, with a step length of roughly 2 mV. The value closest to 0.9 V was always chosen but depending on if the data point lies in the upper or lower parts of the interval 0.9 ± 0.001 V, the calculated activity could vary. For the two best coatings of the three mentioned earlier, with MAs 91 and 77 $\mathrm{mA/mg_{Pt}}$, their ORR curves seem to be shifted with about 5 mV around 0.9 V. The choice of exact data point seems to be part of the difference in MA, but not the only reason.

Continuing the analysis of possible errors, the errors of the SA differ from the errors than the MA. The SA is dependent on both ECSA and activity measurements, meaning uncertainties in the measurements are amplified for the SA. The MA on the other hand, can be affected by assuming the wrong mass of platinum in the coating. As mentioned earlier, this can be caused by errors in the ink preparation since the amount of catalyst used is very small, but it could also occur due to small variations in the amount of ink deposited on the GC. If the ink deposited is 10.0 ± 0.2 µl, the error is however quite small and probably negligible to other uncertainties such as the quality of the coating. An error in the mass of platinum is most likely proportional to the resulted error in the ECSA or MA.

5

Conclusion

This work studies the influence of IPA content, Pt loading and pH of catalyst inks used with the RDE method. When the IPA content was varied for catalyst A, no significant changes in the measured activity were observed in either magnitude or variation between measurements. A lower IPA content made the ink spread out less which was easier to work with but also required more effort in getting the catalyst to cover the entire GC disk and reach the theoretical diffusion limited current. The conclusion is that catalyst A is not very sensitive to changes in IPA content, a sensitivity which might be related to the catalyst's hydrophobicity.

Regarding the Pt loading, there exists a lower limit where the catalyst is not able to form a homogeneous coating. This resulted in a less negative diffusion limited current as well as a lower SA. For catalyst A, this lower limit is in the range of $10 - 20\,\mu g_{Pt}/cm^2$. There probably exists an upper limit as well where the coating becomes too thick, but to find this limit for catalyst A, more research is needed. The limit is at least above $34.8\,\mu g_{Pt}/cm^2$ since this loading produced similar results as $19.9\,\mu g_{Pt}/cm^2$. To conclude, catalyst A is able to produce good coatings in at least the range $19.9 - 34.8\,\mu g_{Pt}/cm^2$.

Catalyst B was tested with different IPA contents and different pH levels. In contrast to catalyst A, it suffered from stability issues, making it difficult to compare inks with different IPA contents. Perhaps the dispersion would be better with even higher than 25 vol% IPA, the highest IPA content tested, but then there will probably be even more issues with the ink spreading outside of the GC disk. In an attempt to increase stability, KOH was added to increase the pH. This increased both coating quality and stability but the coating quality was still not as good as coatings with catalyst A. Adding KOH also appears to have a positive effect on the ORR activity but the difference is small and more experiments would be needed to draw a more certain conclusion.

5.1 Outlook

Based on the findings of this thesis, it is clear that there is still progress to be made in achieving reliable results of the ORR activity with the RDE method. This is especially true for catalyst B, for which a homogenous coating was not achieved in this work.

For some ink recipes with catalyst A, the results differed a lot between the two inks made and should therefore be redone to test whether the results are valid or a result of some error. This is especially true for the ink with 21.5 vol% IPA where one ink had a surprisingly low activity with no reasonable explanation at the moment. Additionally, due to the coatings dependence on nitrogen flow during drying, one could further investigate how the rate, height and angle of the flow should be optimized to improve reproducibility. Furthermore, the reproducibility of coatings could be improved by exploring automation of the coating procedure.

Further investigations are needed to understand the effect of KOH on the ORR activity. The number of samples in Table 4.1 is quite small and since the difference in ORR activity is small, it is unsure if this difference is real or just a coincidence. Additionally, the coatings without KOH were of low quality and maybe the activity would have been different if the ink had been newer, something which should be investigated. To increase the homogeneity further, studying the solvent might be of interest since it might lead to a better ink dispersion. An even higher IPA content could be tested, though a smaller aliquot of ink on the GC disk would probably be required. Another idea could be to test other solvents, for example ethanol, or vary the I/C ratio to improve the dispersion and stability. The method of dispersion could also be explored, perhaps by changing the energy input or amplitude of the ultrasonic disperser. One could also place the ink vial in an ice bath instead of just cold tap water during dispersion, as suggested by Kocha et al. [20].

References

[1] *The Paris Agreement | UNFCCC*. [Online]. Available: https://unfccc.int/process-and-meetings/the-paris-agreement.

[2] G. G. Scherer, "Fuel Cell Types and Their Electrochemistry", in *Fuel Cells and Hydrogen Production: A Volume in the Encyclopedia of Sustainability Science and Technology, Second Edition*, T. E. Lipman and A. Z. Weber, Eds., New York, NY: Springer New York, 2019, pp. 83–98, ISBN: 978-1-4939-7789-5. DOI: 10.1007/978-1-4939-7789-5{_}132. [Online]. Available: https://doi.org/10.1007/978-1-4939-7789-5_132.

[3] F. Barbir, "CHAPTER 1 - Introduction", in *PEM Fuel Cells*, F. Barbir, Ed., Burlington: Academic Press, 2005, pp. 1–16, ISBN: 978-0-12-078142-3. DOI: https://doi.org/10.1016/B978-012078142-3/50002-1. [Online]. Available: https://www.sciencedirect.com/science/article/pii/B9780120781423500021.

[4] A. de Frank Bruijn and G. J. M. Janssen, "PEM Fuel Cell Materials: Costs, Performance, and Durability", in *Fuel Cells and Hydrogen Production: A Volume in the Encyclopedia of Sustainability Science and Technology, Second Edition*, T. E. Lipman and A. Z. Weber, Eds., New York, NY: Springer New York, 2019, pp. 195–234, ISBN: 978-1-4939-7789-5. DOI: 10.1007/978-1-4939-7789-5{_}152. [Online]. Available: https://doi.org/10.1007/978-1-4939-7789-5_152.

[5] Y. Lv, H. Liu, J. Li, J. Chen, and Y. Song, "A convenient protocol for the evaluation of commercial Pt/C electrocatalysts toward oxygen reduction reaction", *Journal of Electroanalytical Chemistry*, vol. 870, p. 114 172, Aug. 2020, ISSN: 1572-6657. DOI: 10.1016/J.JELECHEM.2020.114172.

[6] Y. Garsany, O. A. Baturina, K. E. Swider-Lyons, and S. S. Kocha, "Experimental Methods for Quantifying the Activity of Platinum Electrocatalysts for the Oxygen Reduction Reaction", *Analytical Chemistry*, vol. 82, no. 15, pp. 6321–6328, Aug. 2010, ISSN: 0003-2700. DOI: 10.1021/ac100306c.

[7] S. Kocha, B. Pivovar, and T. Gennett, "Fuel cells", in *Fundamentals of Materials for Energy and Environmental Sustainability*, Cambridge University Press, Jan. 2011, pp. 637–655, ISBN: 9780511718786. DOI: 10.1017/CBO9780511718786.053.

[8] D. Pletcher, *A First Course in Electrode Processes*. The Royal Society of Chemistry, Aug. 2009, ISBN: 978-1-84755-893-0. DOI: 10.1039/9781839169083. [Online]. Available: https://doi.org/10.1039/9781839169083.

[9] F. Barbir, "CHAPTER 2 - Fuel Cell Basic Chemistry and Thermodynamics", in *PEM Fuel Cells*, F. Barbir, Ed., Burlington: Academic Press, 2005, pp. 17–32, ISBN: 978-0-12-078142-3. DOI: https://doi.org/10.1016/B978-012078142-3/50003-3. [Online]. Available: https://www.sciencedirect.com/science/article/pii/B9780120781423500033.

[10] C. Di Paola *et al.*, "Platinum-based catalysts for oxygen reduction reaction simulated with a quantum computer", *npj Computational Materials 2024 10:1*, vol. 10, no. 1, pp. 1–10, Dec. 2024, ISSN: 2057-3960. DOI: 10.1038/s41524-024-01460-x. [Online]. Available: https://www.nature.com/articles/s41524-024-01460-x.

[11] F. Barbir, "CHAPTER 3 - Fuel Cell Electrochemistry", in *PEM Fuel Cells*, F. Barbir, Ed., Burlington: Academic Press, 2005, pp. 33–72, ISBN: 978-0-12-078142-3. DOI: https://doi.org/10.1016/B978-012078142-3/50004-5. [Online]. Available: https://www.sciencedirect.com/science/article/pii/B9780120781423500045.

[12] J. Hou *et al.*, "Platinum-group-metal catalysts for proton exchange membrane fuel cells: From catalyst design to electrode structure optimization", *EnergyChem*, vol. 2, no. 1, p. 100 023, Jan. 2020, ISSN: 2589-7780. DOI: 10.1016/J.ENCHEM.2019.100023. [Online]. Available: https://www.sciencedirect.com/science/article/abs/pii/S2589778019300260.

[13] M. M. Rahman *et al.*, "Synthesis of catalysts with fine platinum particles supported by high-surface-area activated carbons and optimization of their catalytic activities for polymer electrolyte fuel cells", *RSC Advances*, vol. 11, no. 33, pp. 20 601–20 611, Jun. 2021, ISSN: 2046-2069. DOI: 10.1039/D1RA02156G. [Online]. Available: https://pubs.rsc.org/en/content/articlehtml/2021/ra/d1ra02156g.

[14] J. Zhao, Z. Tu, and S. H. Chan, "Carbon corrosion mechanism and mitigation strategies in a proton exchange membrane fuel cell (PEMFC): A review", *Journal of Power Sources*, vol. 488, p. 229 434, Mar. 2021, ISSN: 0378-7753. DOI: 10.1016/J.JPOWSOUR.2020.229434. [Online]. Available: https://www.sciencedirect.com/science/article/pii/S0378775320317171.

[15] S. Chen, "Practical Electrochemical Cells", *Handbook of Electrochemistry*, pp. 33–56, Jan. 2007. DOI: 10.1016/B978-044451958-0.50003-3.

[16] G. Jerkiewicz, "Standard and Reversible Hydrogen Electrodes: Theory, Design, Operation, and Applications", *ACS Catalysis*, vol. 10, no. 15, pp. 8409–8417, Aug. 2020, ISSN: 21555435. DOI: 10.1021/ACSCATAL.0C02046/ASSET/IMAGES/LARGE/CS0C02046{_}0008.JPEG. [Online]. Available: /doi/pdf/10.1021/acscatal.0c02046.

[17] G. Denuault, M. Sosna, and K. J. Williams, "Classical Experiments", *Handbook of Electrochemistry*, pp. 431–469, Jan. 2007. DOI: 10.1016/B978-044451958-0.50024-0.

[18] M. K. Puglia and P. K. Bowen, "Cyclic Voltammetry Study of Noble Metals and Their Alloys for Use in Implantable Electrodes", *ACS Omega*, vol. 7, no. 38, pp. 34 200–34 212, Sep. 2022, ISSN: 24701343. DOI: 10.1021/ACSOMEGA.2C03563/ASSET/IMAGES/LARGE/AO2C03563{_}0011.JPEG. [Online]. Available: https://pubs.acs.org/doi/full/10.1021/acsomega.2c03563.

[19] W. Zheng, "iR Compensation for Electrocatalysis Studies: Considerations and Recommendations", *ACS Energy Letters*, vol. 8, no. 4, pp. 1952–1958, Apr. 2023, ISSN: 23808195. DOI: 10.1021/ACSENERGYLETT.3C00366/ASSET/IMAGES/LARGE/NZ3C00366{_}0005.JPEG. [Online]. Available: https://pubs.acs.org/doi/full/10.1021/acsenergylett.3c00366.

[20] S. S. Kocha *et al.*, "Best Practices and Testing Protocols for Benchmarking ORR Activities of Fuel Cell Electrocatalysts Using Rotating Disk Electrode", *Electrocatalysis*, vol. 8, no. 4, pp. 366–374, Jul. 2017, ISSN: 18685994. DOI: 10.1007/S12678-017-0378-6/TABLES/8. [Online]. Available: https://link.springer.com/article/10.1007/s12678-017-0378-6.

[21] Y. Garsany, J. Ge, J. St-Pierre, R. Rocheleau, and K. E. Swider-Lyons, "Analytical Procedure for Accurate Comparison of Rotating Disk Electrode Results for the Oxygen Reduction Activity of Pt/C", *Journal of The Electrochemical Society*, vol. 161, no. 5, F628–F640, Mar. 2014, ISSN: 0013-4651. DOI: 10.1149/2.036405jes.

[22] K. Nagasawa *et al.*, "Performance and durability of Pt/C cathode catalysts with different kinds of carbons for polymer electrolyte fuel cells characterized by electrochemical and in situ XAFS techniques", *Physical Chemistry Chemical Physics*, vol. 16, no. 21, pp. 10 075–10 087, May 2014, ISSN: 1463-9084. DOI: 10.1039/C3CP54457E. [Online]. Available: https://pubs.rsc.org/en/content/articlehtml/2014/cp/c3cp54457e.

[23] K. J. Mayrhofer, D. Strmcnik, B. B. Blizanac, V. Stamenkovic, M. Arenz, and N. M. Markovic, "Measurement of oxygen reduction activities via the rotating disc electrode method: From Pt model surfaces to carbon-supported high surface area catalysts", *Electrochimica Acta*, vol. 53, no. 7, pp. 3181–3188, Feb. 2008, ISSN: 00134686. DOI: 10.1016/j.electacta.2007.11.057.

[24] M. Jaroniec, M. Kruk, and A. Sayari, "Adsorption methods for characterization of surface and structural properties of mesoporous molecular sieves", *Studies in Surface Science and Catalysis*, vol. 117, pp. 325–332, Jan. 1998, ISSN: 0167-2991. DOI: 10.1016/S0167-2991(98)81008-2. [Online]. Available: https://www.sciencedirect.com/science/article/pii/S0167299198810082.

[25] H. Wang, A. S. Adeleye, Y. Huang, F. Li, and A. A. Keller, "Heteroaggregation of nanoparticles with biocolloids and geocolloids", *Advances in Colloid and Interface Science*, vol. 226, pp. 24–36, Dec. 2015, ISSN: 0001-8686. DOI: 10.1016/J.CIS.2015.07.002. [Online]. Available: https://www.sciencedirect.com/science/article/pii/S0001868615000949.

[26] P. Liu *et al.*, "Agglomeration behavior of carbon-supported platinum nanoparticles in catalyst ink: modeling and experimental investigation", *Journal of Power Sources*, vol. 602, p. 234 309, May 2024, ISSN: 0378-7753. DOI: 10.1016/J.JPOWSOUR.2024.234309. [Online]. Available: https://www.sciencedirect.com/science/article/pii/S037877532400260X.

[27] M. Inaba, J. Quinson, and M. Arenz, "pH matters: The influence of the catalyst ink on the oxygen reduction activity determined in thin film rotating disk electrode measurements", *Journal of Power Sources*, vol. 353, pp. 19–27, 2017, ISSN: 03787753. DOI: 10.1016/j.jpowsour.2017.03.140.

[28] S. Khandavalli *et al.*, "Rheological Investigation on the Microstructure of Fuel Cell Catalyst Inks", *ACS Applied Materials and Interfaces*, vol. 10, no. 50, pp. 43 610–43 622, Dec. 2018, ISSN: 19448252. DOI: 10.1021/ACSAMI.8B15039/SUPPL{_}FILE/AM8B15039{_}SI{_}001.PDF. [Online]. Available: /doi/pdf/10.1021/acsami.8b15039.

[29] K. Shinozaki, J. W. Zack, S. Pylypenko, B. S. Pivovar, and S. S. Kocha, "Oxygen Reduction Reaction Measurements on Platinum Electrocatalysts Utilizing Rotating Disk Electrode Technique", *Journal of The Electrochemical Society*, vol. 162, no. 12, F1384–F1396, 2015, ISSN: 0013-4651. DOI: 10.1149/2.0551512jes.

[30] I. Takahashi and S. S. Kocha, "Examination of the activity and durability of PEMFC catalysts in liquid electrolytes", *Journal of Power Sources*, vol. 195, no. 19, pp. 6312–6322, Oct. 2010, ISSN: 03787753. DOI: 10.1016/j.jpowsour.2010.04.052.

[31] K. Ke, K. Hiroshima, Y. Kamitaka, T. Hatanaka, and Y. Morimoto, "An accurate evaluation for the activity of nano-sized electrocatalysts by a thin-film rotating disk electrode: Oxygen reduction on Pt/C", *Electrochimica Acta*, vol. 72, pp. 120–128, Jun. 2012, ISSN: 00134686. DOI: 10.1016/j.electacta.2012.04.004.

[32] M. Inaba, Y. Kamitaka, and K. Kodama, "Eliminating the need for craftsmanship: Facile and precise determination of oxygen reduction reaction activity by spraying catalyst ink on rotating disk electrode", *Journal of Electroanalytical Chemistry*, vol. 886, Apr. 2021, ISSN: 15726657. DOI: 10.1016/j.jelechem.2021.115115.

[33] Y. Garsany, I. L. Singer, and K. E. Swider-Lyons, "Impact of film drying procedures on RDE characterization of Pt/VC electrocatalysts", *Journal of Electroanalytical Chemistry*, vol. 662, no. 2, pp. 396–406, Nov. 2011, ISSN: 15726657. DOI: 10.1016/j.jelechem.2011.09.016.

A

Results of individual coatings

The results for ECSA, MA and SA for each measurment with catalyst A are presented in Tables A.1 and A.2. These results are used to calculate the mean values and standard deviations that are presented in Figures 4.2, 4.3, 4.6 and 4.7.

Table A.1: Results from RDE measurements for coatings from inks with different alcohol contents.

Ink	**Alcohol** [vol%]	m_{Pt} [µg]	**ECSA** [m^2/g]	i [mA]	i_d [mA]	i_k [mA]	**MA** [mA/mg_{Pt}]	**SA** [$\mu A/cm^2_{Pt}$]
1	11.2	3.82	55	−0.243	−0.957	−0.326	85	154
1	11.2	3.82	56	−0.240	−1.01	−0.316	83	147
1	11.2	3.82	50	−0.222	−1.14	−0.276	72	143
1	11.2	3.82	51	−0.202	−1.05	−0.250	65	127
2	11.1	3.91	60	−0.222	−1.12	−0.277	72	121
2	11.1	3.91	75	−0.386	−1.13	−0.586	153	204
2	11.1	3.82	60	−0.302	−1.13	−0.413	108	181
2	11.1	3.82	61	−0.310	−1.17	−0.421	110	180
3	19.1	3.82	74	−0.298	−1.17	−0.400	102	138
3	19.1	3.82	73	−0.306	−1.17	−0.415	106	145
4	19.3	3.91	66	−0.274	−1.16	−0.358	91	139
4	19.3	3.91	60	−0.321	−1.20	−0.438	112	187
4	19.3	3.91	66	−0.316	−1.14	−0.438	112	170
5	21.4	3.84	67	−0.236	−1.15	−0.297	77	115
5	21.4	3.84	65	−0.269	−1.15	−0.351	91	140
5	21.4	3.84	65	−0.236	−1.15	−0.297	77	119
6	21.5	3.88	68	−0.284	−1.19	−0.374	96	141
6	21.5	3.88	69	−0.316	−1.21	−0.428	110	160

Table A.2: Results from RDE measurements for coatings from inks with different platinum loadings.

Ink	Pt loading [$\mu g_{Pt}/cm^2$]	m_{Pt} [µg]	ECSA [m^2/g]	i [mA]	i_d [mA]	i_k [mA]	MA [mA/mg_{Pt}]	SA [$\mu A/cm^2_{Pt}$]
3	19.9	3.82	74	−0.298	−1.17	−0.400	102	138
3	19.9	3.82	73	−0.306	−1.17	−0.415	106	145
4	19.9	3.91	66	−0.274	−1.16	−0.358	91	139
4	19.9	3.91	60	−0.321	−1.20	−0.438	112	187
4	19.9	3.91	66	−0.316	−1.14	−0.438	112	170
8	34.8	6.828	69	−0.431	−1.15	−0.691	101	148
8	34.8	6.828	67	−0.471	−1.17	−0.788	115	173
8	34.8	6.828	66	−0.498	−1.15	−0.876	128	194
9	34.8	6.828	70	−0.438	−1.17	−0.701	103	147
9	34.8	6.828	69	−0.453	−1.20	−0.727	106	154
10	10.0	1.968	109	−0.215	−1.16	−0.264	134	122
10	10.0	1.968	109	−0.218	−1.14	−0.269	137	125
10	10.0	1.968	110	−0.265	−1.14	−0.345	176	160
11	10.0	1.966	67	−0.136	−1.07	−0.156	79	118
11	10.0	1.966	66	−0.134	−1.00	−0.154	78	118
11	10.0	1.966	65	−0.143	−1.04	−0.166	85	129

DEPARTMENT OF SOME SUBJECT OR TECHNOLOGY
CHALMERS UNIVERSITY OF TECHNOLOGY
Gothenburg, Sweden
www.chalmers.se

CHALMERS
UNIVERSITY OF TECHNOLOGY